Article

Current Biology

Minute-encoding neurons in hippocampal-striatal circuits

Graphical Abstract

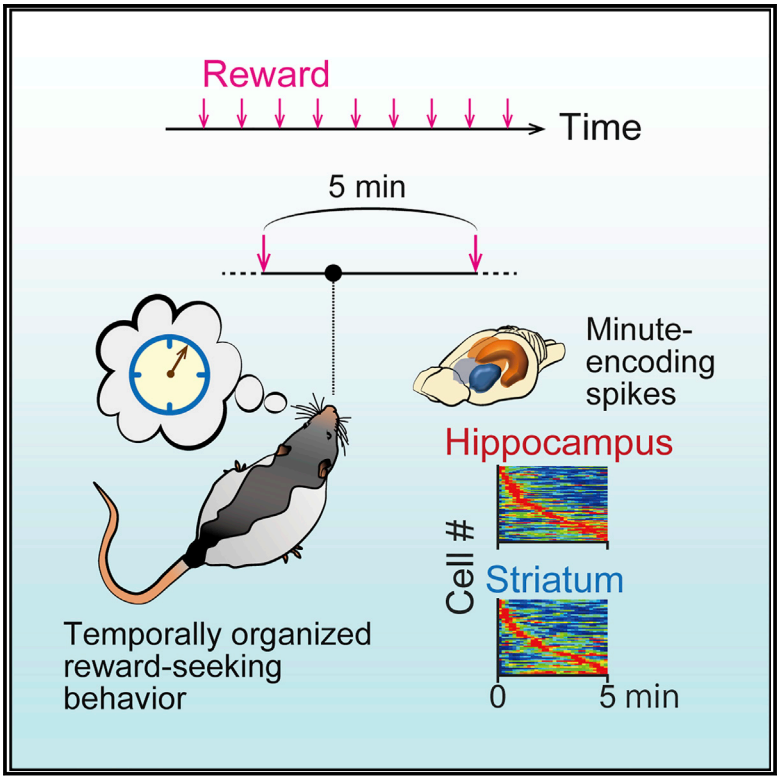

Highlights

- Animals change their reward-seeking behavior over minutes for future reward
- Hippocampal and striatal neurons encode time on the order of minutes
- Striatal minute-encoding patterns depend on hippocampal activity
- Minute-encoding representation develops with animals' experience

Authors

Yu Shikano, Yuji Ikegaya, Takuya Sasaki

Correspondence

tsasaki@mol.f.u-tokyo.ac.jp

In Brief

Using a hippocampus-dependent behavioral task in which rats need to wait for reward presentation for several minutes, Shikano et al. demonstrate that hippocampal and striatal neurons encode elapsed time in the range of minutes. These results suggest a neuronal basis for temporal information processing and formation of episodic memory over minutes.

Shikano et al., 2021, Current Biology *31*, 1–12
April 12, 2021
https://doi.org/10.1016/j.cub.2021.01.032

CellPress

Current Biology

CellPress

Article

Minute-encoding neurons in hippocampal-striatal circuits

Yu Shikano,[1] Yuji Ikegaya,[1,2,3] and Takuya Sasaki[1,4,5,*]

[1]Graduate School of Pharmaceutical Sciences, The University of Tokyo, 7-3-1 Hongo, Bunkyo-ku, Tokyo 113-0033, Japan
[2]Center for Information and Neural Networks, 1-4 Yamadaoka, Suita City, Osaka 565-0871, Japan
[3]Institute for AI and Beyond, The University of Tokyo, Tokyo 113-0033, Japan
[4]Precursory Research for Embryonic Science and Technology (PRESTO), Japan Science and Technology Agency (JST), 4-1-8 Honcho, Kawaguchi, Saitama 332-0012, Japan
[5]Lead contact
*Correspondence: tsasaki@mol.f.u-tokyo.ac.jp
https://doi.org/10.1016/j.cub.2021.01.032

SUMMARY

Animals process temporal information in an ever-changing environment, but the neuronal mechanisms of this process, especially on timescales longer than seconds, remain unresolved. Here, we designed a hippocampus-dependent task in which rats prospectively increased their reward-seeking behavior over a duration of minutes. During this timing behavior, hippocampal and striatal neurons represented successive time points on the order of minutes by gradually changing their firing rates and transiently increasing their firing rates at specific time points. These minute-encoding patterns progressively developed as the rats learned a time-reward relationship, and the patterns underwent flexible scaling in parallel with timing behavior. These observations suggest a neuronal basis in the hippocampal-striatal circuits that enables temporal processing and formation of episodic memory on a timescale of minutes.

INTRODUCTION

Living organisms must recognize time at various temporal scales to create episodic-like memory and to properly execute future actions. While the hippocampal and striatal circuits have been implicated as core brain regions for temporal information processing, including time perception and estimation,[1–7] the detailed neurophysiological mechanisms remain poorly understood.

Recent works have proposed several behavioral tasks in which rodent animals repeatedly experience a temporal context and demonstrated that hippocampal and striatal neurons robustly encode elapsed time over durations of tens of seconds,[8–20] as typically represented by hippocampal time cells.[13,15,19,20] These spike patterns are considered to enable a time-keeping function to retain working memory and anticipate future outcomes in the range of seconds.

A further challenging issue is whether the rodent brain can process temporal information at timescales exceeding seconds. Some early studies have shown that rodent animals can take appropriate behavioral patterns according to elapsed time in the range of minutes.[21,22] In various natural situations, their ability of temporal information processing on the order of minutes should be crucial to achieve appropriate interval timing behavior, e.g., in foraging and decision making. However, neuronal mechanisms underlying such minute-range behavior remain unclear.

As this timescale is considerably longer than the millisecond resolution of neuronal spikes and neurotransmission, neuronal encoding of minutes may not be simply explained by the sequential accumulation of temporally organized spike patterns in the milliseconds-to-seconds range. Instead, for the encoding of longer timescales such as hours and days, continuous drifting of active hippocampal neuronal ensembles has been suggested as a neuronal substrate to allow animals to keep track of the passage of time and support the temporal organization of episodic memories.[20,23–28] Crucially, these temporal changes in activity have been observed in animals that were possibly unaware of the progression of time, as they were not trained in any task that specifically demanded temporal cognition.

There remains a question regarding whether neurons robustly process temporal information in the range of minutes and whether their temporal tuning patterns. Here, we designed a behavioral task in which rats needed to learn to attend the passage of minutes to efficiently obtain a reward every 5 min. The rats adaptively increased the behavior of checking inside a reward port, which served as an explicit behavioral sign of internal time estimation. From animals engaging in such reproducible behavior over minutes, we recorded spike patterns of neuronal populations in the dorsal hippocampus and dorsal striatum.

RESULTS

Five-min task

Rats performed a 5-min task in which they consumed a 45-mg reward pellet presented from a feeding port located in one corner of a test box (25 cm × 25 cm) every 5 min (Figures 1A and S1A). In this small recording box, the animals' moving space was tightly restricted (Figures S1F and S1H). Pellet dispensation

Please cite this article in press as: Shikano et al., Minute-encoding neurons in hippocampal-striatal circuits, Current Biology (2021), https://doi.org/10.1016/j.cub.2021.01.032

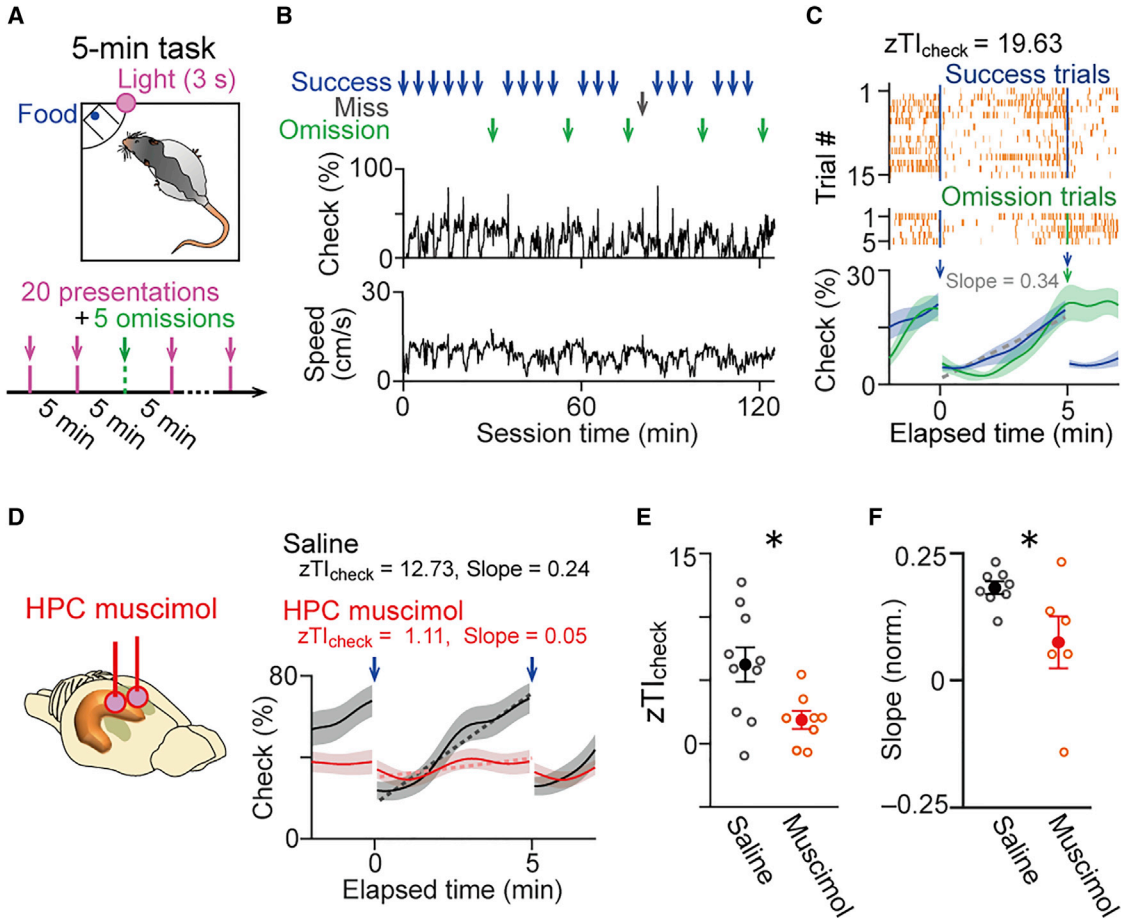

Figure 1. Behavioral patterns in the 5-min task

(A) Schematic illustration of the 5-min task.

(B) The percentage of checking behavior and running speed (bin = 20 s) in a session. Each arrow above represents a pellet presentation (blue, success; gray, miss; green, omission).

(C) (Top) Raster plots showing the timing of checking behavior aligned to trial onset, separately plotted for success and omission trials. (Bottom) Average percentages of checking behavior across the trials. The gray dotted line indicates the regression line computed from the tuning curve in success trials. Success trials, $F_{28,392} = 13.24$, $p = 3.1 \times 10^{-41}$, one-way repeated-measures ANOVA. Omission trials, $F_{28,112} = 4.46$, $p = 7.1 \times 10^{-9}$.

(D) Effects of bilateral injection of saline (black) and muscimol (red) into the dorsal hippocampus on checking behavior in a representative rat. The dotted lines represent the regression lines for the tuning curves.

(E) Summary of zTI$_{check}$ in all rats (saline, n = 10 sessions from 4 rats; muscimol, n = 8 sessions from 4 rats). Each dot represents each session. Data are mean ± SEM. *$p < 0.05$, Student's t test.

(F) Summary of regression slopes of behavioral tuning curves (saline, n = 8 sessions with significant slopes from 4 rats; muscimol, n = 6 sessions with significant slopes from 3 rats). Each dot represents each session. Data are mean ± SEM. *$p < 0.05$, Student's t test. See also Figure S1.

was regulated by a rotating feeding wheel (Figure S1A). The onset of pellet dispensation generated a small ticking sound, serving as an auditory cue signal. A light-emitting diode (LED) was illuminated during the 3 s pellet presentation periods as a visual cue signal. If the pellets were not consumed by the rats during the 3 s presentation periods, the pellets were removed by the feeding wheel. Each pellet presentation lasted for only 3 s and was classified as a success or a miss event (Figure 1B). All rats took less than 8 s (on average, 5.7 ± 0.3 s) to complete the chewing behavior (Figure S1J). Each session consisted of 20 pellet presentations and up to 5 omissions (no pellet presented) in a random order. A single trial was defined as the period from the end of a success event to the subsequent pellet presentation 5 min later. The percentage of success trials was 94.2% ± 1.2% (n = 44 sessions from 12 rats). The average running speed in the 5-min task was 4.3 ± 0.2 cm/s (Figures 1B and S1H). During the task, the rats occasionally peeked into the port (Figures S1A and S1J) in what we termed checking behavior, which potentially reflected reward-seeking behavior. The probability of checking behavior changed over time during the 5-min intervals (Figure 1C; $F_{29,928} = 94.36$, $p = 4.6 \times 10^{-11}$, repeated-measures ANOVA for all rats) and rapidly dropped immediately after success events (Figure S1D) but not after omission events (Figure S1E). In the following analyses, only success trials were analyzed, unless otherwise specified. To quantify time changes in checking behavior across time, we computed two measures, temporal information (TI$_{check}$) and a regression coefficient. A TI$_{check}$ value was computed from a temporal tuning curve

Please cite this article in press as: Shikano et al., Minute-encoding neurons in hippocampal-striatal circuits, Current Biology (2021), https://doi.org/10.1016/j.cub.2021.01.032

(bin = 10 s) of checking behavior in each session. To evaluate the significance of TI_{check} in the original data, we created shuffled data in which the timing of checking behavior was randomized while maintaining the total duration of checking behavior in each trial. This randomization was repeated 1,000 times, yielding the distribution of TI_{check} from 1,000 shuffled datasets. For an original TI_{check} value, a *Z*-scored TI_{check} (zTI_{check}) value was computed based on the average and standard deviation (SD) of the distribution (Figures 1C, S1B, and S1C). A zTI_{check} value greater than 2.33 ($p < 0.01$) was considered significant (individual rats shown in Figure S1C, n = 44 sessions from 12 rats). From the same temporal tuning curve, a regression line was computed by linear fitting. In all 44 sessions from 12 rats tested, 84.1% of sessions had significantly positive slopes (Figure S1C). These results demonstrate that the rats increase their checking behavior over the course of minutes during the 5-min intervals, ensuring their recognition of task requirements and expectation of time until reward delivery at behavioral levels.

The contribution of the hippocampus to temporal changes in checking behavior was tested by inactivating the bilateral dorsal hippocampus with muscimol (Figure 1D). Of 13 and 9 sessions, 3 and 1 sessions with average check rates less than 3.3% (10 s per trial) were excluded from the following checking behavior analyses, respectively. Hippocampal muscimol administration significantly decreased both zTI_{check} and slopes of changes in checking behavior (Figure 1E; zTI_{check}, n = 10 sessions from 4 rats and n = 8 sessions from 4 rats, respectively, $t_{16} = 2.63$, $p = 0.018$; Figure 1F; slope: n = 8 sessions with significant slopes from 4 rats and n = 6 sessions with significant slopes from 3 rats, respectively, $t_{12} = 2.34$, $p = 0.038$, Student's t test). In addition, the number of miss events was significantly increased in hippocampal muscimol-injected rats (Figure S1I). These results establish that the temporal increases in checking behavior in this task are hippocampus dependent.

Minute encoding by hippocampal cells

Spike patterns were recorded from 313 neurons in the dorsal hippocampal CA1 (HPC) region as the rats performed the 5-min task (n = 24 sessions from 10 rats; Figures 2A, 2B, and S2A). In each neuron, instantaneous firing-rate changes (bin = 10 s, a Gaussian filter with a SD of 1 [10 s]) aligned to trial onset are computed in individual trials and a spike-rate temporal tuning curve was obtained by averaging the firing-rate changes over all trials in each bin (Figures 2C and S2B–S2D; all tuning curves are shown as the mean ± SEM). Some hippocampal neurons changed their firing rates with time during the 5-min intervals, implying their ability to encode minutes. However, the other possibility is that such temporal changes are simply due to the strong dependence of hippocampal neuronal spike rates on the rat's locations (e.g., place cells), head directions (e.g., head direction cells), moving speed, and the frequency of checking behavior. Here, we statistically compensated for these minor behavioral variations across time using the linear-nonlinear-Poisson (LN) model,[29] which extracted pure time-dependent changes in spike rates. From an LN model-adjusted temporal tuning curve in each neuron (orange traces in Figures 2C, S2B, and S2D), the *Z*-scored temporal information of spikes (zTI_{spike}) was computed by creating the corresponding 100 shuffled tuning curves from the same datasets in which all interspike intervals were randomly shuffled in each trial. This analytical procedure was basically similar to that for computing zTI_{check} as described before. A hippocampal minute-encoding neuron was defined as a neuron with zTI_{spike} greater than 2.33 (99% confidence) and an average firing rate ranging from 0.1 to 3 Hz (Figure 3A; 23.3%; n = 73 out of 313 cells). In omission trials, the temporal tuning curves of minute-encoding neurons during the 5-min intervals were almost identical to those in success trials (Figures S3A and S3B), but their temporal patterns significantly differed in the next 5-min periods (Figure S3D), confirming that temporal tuning of spike rates over 5 min was not reproducible when omission events occurred.

Time-encoding patterns are accounted for by two firing types: (1) a "ramping-up/down" firing type, showing monotonic increases/decreases in spike rates throughout a time interval, as demonstrated by the integration of time signals observed from lateral entorhinal neurons,[30] and (2) a "specific peak" firing type, responding to specific time points within a brief window, as demonstrated by spike patterns of second-range "time cells."[13] To estimate whether spike-rate changes showed ramping across time, a regression line was computed by linearly fitting the baseline (taken as the bottom 50% to exclude the effect of a specific peak, if any) of an LN model-adjusted temporal tuning curve in each minute-encoding neuron (Figures 2C, dotted lines, and 3B, x axis). Minute-encoding neurons with a p value less than 0.05 in the regression were considered significant and classified as a ramping firing type. Based on this criterion, 27.4% (20 out of 73) and 26.0% (19 out of 73) of minute-encoding neurons were identified as ramping up and down types, respectively (Figure 3C). To determine whether spike-rate changes during the 5-min interval had a specific peak, a ridge-to-background (RB) ratio was computed[31,32] (Figures 2C and 3B, y axis). When a neuron was classified as a ramping firing type, its RB ratio was calculated from a tuning curve after subtracting the regression line from the LN model-adjusted temporal tuning curve. The significance of the RB ratio was evaluated by computing a *Z*-scored RB ratio (zRB ratio) based on the average and SD of RB ratios computed from the corresponding 100 shuffled tuning curves. Minute-encoding neurons with a zRB ratio greater than 2.33 ($p < 0.01$) were considered significant and classified as a specific peak firing type. Out of the 73 minute-encoding neurons, 34 (46.6%) neurons were identified as a specific peak firing type. Overall, 20 (27.4%) neurons were determined to contain both ramping and specific peak firing types, and 20 (27.4%) neurons were classified into neither type. For neurons classified as a specific peak firing type, there was a significantly positive correlation between the time at peak firing and the width of the time fields (Figure 3D; only fields that ended before the end of trials; n = 31 neurons, $r = 0.38$, $p = 0.034$; Pearson correlation coefficient).

We next tested the possibility that these tuning curves of minute-encoding neurons successively tiled entire periods across the 5-min interval. The normalized temporal tuning curves of all hippocampal minute-encoding neurons are shown in Figure 3E. No significant changes in average normalized modulation indexes were observed during the 5-min interval (Figure 3E, bottom; $p > 0.05$, Tukey's test). Next, a sequentiality index (SI) was computed from the pooled data from all minute-encoding neurons as the sum of the entropy of the peak firing time distribution of minute-encoding neurons and the average logarithm

Please cite this article in press as: Shikano et al., Minute-encoding neurons in hippocampal-striatal circuits, Current Biology (2021), https://doi.org/10.1016/j.cub.2021.01.032

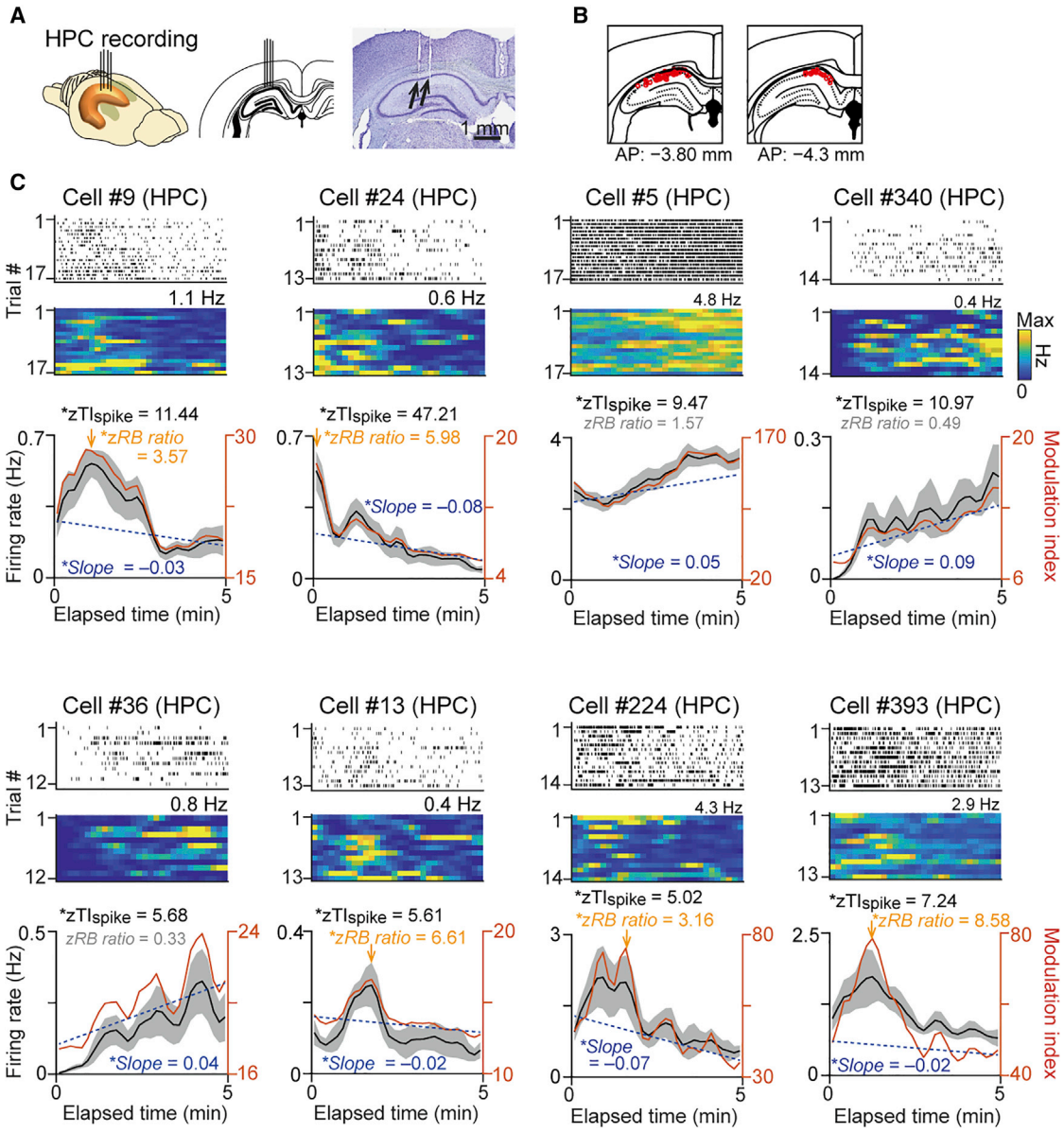

Figure 2. Minute encoding by hippocampal neurons

(A) Multiunit recordings were performed from the dorsal hippocampal CA1 region (HPC), as indicated by arrows on a coronal section.

(B) Superimpositions of recording sites for all 69 tetrodes from 18 rats, as indicated by red dots on coronal brain sections.

(C) Eight representative minute-encoding neurons in the hippocampus. Each panel shows, from top to bottom, a raster plot showing spike patterns aligned to trial onset, the corresponding pseudocolor image showing instantaneous firing rates (bin = 10 s; blue and yellow represent zero and the peak firing rate described above, respectively), and the temporal tuning curve averaged over all trials (black and gray, original mean and SEM, respectively; orange, adjusted by the LN model). The dotted line represents the regression line fitted to the baseline of the LN model-adjusted temporal tuning curve. The slopes of neurons classified as a ramping firing type are labeled in blue. The yellow arrow above represents the peak time in neurons classified as a specific peak type. See also Figure S2.

of RB ratios of the neurons (Figure S2H).[31] In the original data, the entropy and SI were 3.11 and 4.46, respectively, which were lower than those of the perfect sequential (PS) model. This result was mainly due to the observations that the proportions and the slopes were not perfectly equivalent between ramping-up and -down firing types (Figure 3C), and peak firing time was slightly biased to the initial phase (Figure 3D). In shuffled (SF) datasets with randomized interspike intervals, the entropy was similar to that of the original data (3.12 ± 0.07), but their mean log(*RB ratio*) was 0.97 ± 0.03, and the SI was 4.09 ± 0.08, which were much lower values than those of the original data. These results suggest that the temporal tuning curves of minute-encoding neurons were structurally distributed across time with their ridges not explained by chance.

For comparison, the same analyses were applied to spike datasets reproduced from Pastalkova et al.,[33] where rats ran on a running wheel for 15 s (Figure S4A), and MacDonald et al.,[13] where rats freely moved and waited for a delay period

Please cite this article in press as: Shikano et al., Minute-encoding neurons in hippocampal-striatal circuits, Current Biology (2021), https://doi.org/10.1016/j.cub.2021.01.032

CellPress

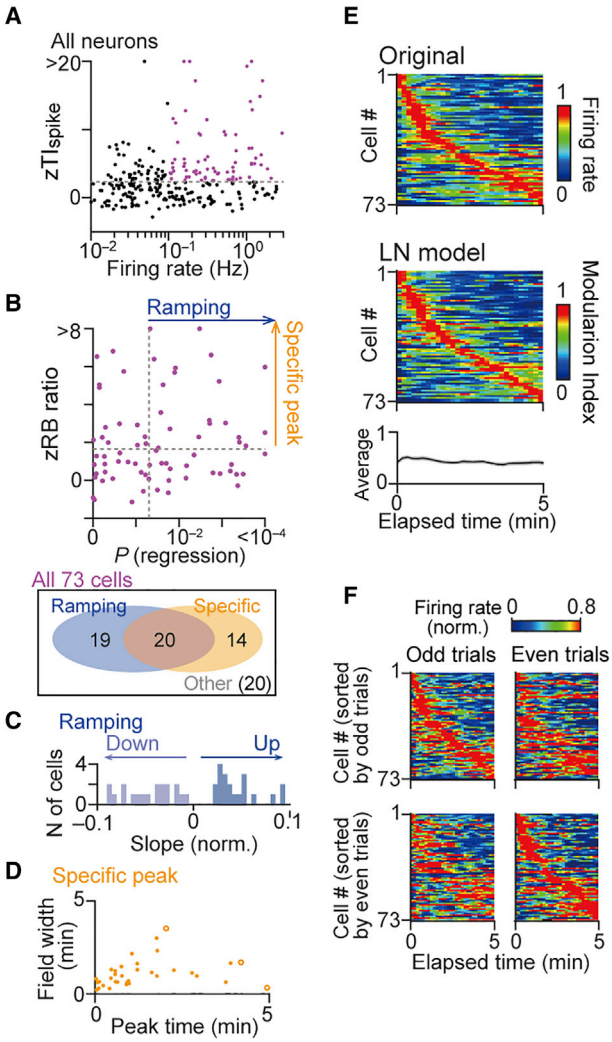

Figure 3. Detailed properties of hippocampal minute-encoding neurons

(A) Relationship between average firing rates and zTI_{spike} of all neurons recorded (n = 313 neurons from 10 rats). Minute-encoding neurons with a firing rate >0.1 Hz and zTI_{spike} >2.33 are labeled in magenta (n = 73 neurons).

(B) (Top) Plots of p values for the linear regression fitted to temporal tuning curves to define a ramping firing type (x axis) and zRB ratios to define a specific peak firing type (y axis). Each dot represents each minute-encoding neuron. (Bottom) Venn diagram showing the number of minute-encoding neurons classified into individual firing types.

(C) Distribution of regression slopes for neurons classified as a ramping firing type (n = 20 ramping-up and 19 ramping-down neurons).

(D) Distribution of time-field widths plotted against the peak time for neurons classified as a specific peak firing type (n = 34 neurons). Each dot represents each neuron. The fields that did not terminate at the end of trials are labeled with open circles and excluded from a correlation analysis. R = 0.38, p = 0.034.

(E) Pseudocolor images showing the original (top) and LN model-adjusted (middle) temporal tuning curves of all minute-encoding hippocampal neurons (n = 73 neurons from 9 rats). The neurons were sorted by their peak times, which correspond to the maximum firing rates, irrespective of their firing types. (Bottom) Average changes in modulation indexes computed from the above LN model-adjusted temporal tuning curves. No significant differences were found across time (p > 0.05). Data are mean ± SEM.

(F) Same as (E) but datasets were depicted from a half of trials (odd or even trials) based on the order of their peak times in a different half of trials.

(G) Bayesian decoding of time from hippocampal spike patterns in a representative rat. To predict time for a target trial (trial #9 or trial #14), the other 10 randomly selected trials were used as a classifier. Heatmap images show posterior probabilities of decoded time plotted against real time, with superimposed blue lines representing the highest probabilities at each time point.

(H) Averaged posterior probabilities over all trials for the rat shown in (G). Posterior probabilities were computed in each trial, and the data from all trials were averaged.

(I) Decoding errors (n = 15 sessions from 8 rats). Blue and black circles represent each session and the average, respectively. The gray horizontal line indicates the chance level computed from shuffled datasets. ***p < 0.001; paired t test. See also Figures S2–S5.

of 5–8 s between discontiguous events (Figure S4B). Second-encoding neurons showed significantly larger zTI_{spike} and zRB ratios than minute-encoding neurons (Figure S4D). In addition, second-encoding neurons classified as a specific peak firing type showed significantly larger differences between peak and baseline firing rates in the tuning curves compared with minute-encoding neurons. The trial-to-trial variability of these spike counts was quantified by computing a coefficient of variation ($CV_{in\text{-}field}$ and CV_{entire}) in each neuron (Figure S4E). The distributions of both $CV_{in\text{-}field}$ and CV_{entire} of the minute-encoding neurons did not significantly differ from those of the second-encoding neurons (Figure S4E).

Elapsed time was decoded from the population spike activity of hippocampal minute-encoding neurons at each time point using a naive Bayesian classifier (Figures 3G–3I and S5A). To compute posterior probability at each time for each trial, a classifier was trained on the other 10 randomly selected trials. Decoded time matched well with true time, as shown by the blue lines in Figures 3G and 3H. To evaluate the decoding performance, we applied the same analysis to the shuffled datasets. Overall, decoding errors in the original datasets were significantly smaller than those in the shuffled datasets (gray horizontal line) (Figure 3I; cells with zTI_{spike} more than 1.04, n = 15 sessions from 8 rats, $t_{14} = -4.58$, $p = 4.3 \times 10^{-4}$, paired t test. Similar successful decoding results were obtained when a classifier was specifically created from the first or the last 8 trials to predict elapsed time in the subsequent or prior trials, respectively (Figure S5C), even while population spike patterns were changed to some extent from the first eight to the last eight trials (Figure S2F).

Please cite this article in press as: Shikano et al., Minute-encoding neurons in hippocampal-striatal circuits, Current Biology (2021), https://doi.org/10.1016/j.cub.2021.01.032

Minute encoding by striatal cells

We next applied the same analyses to spike patterns from 185 neurons in the dorsal striatum (n = 19 sessions from 8 rats; Figures 4A and S2A), a region known to process time information.[8,34,35] Some striatal neurons were also classified as minute-encoding neurons (zTI_{spike} >2.33, an average firing rate between 0.1 and 10 Hz) (Figures 4B–4D and S2E; 27.6%; n = 51 out of 185 cells). Out of the 51 minute-encoding neurons, 45.1% (23 out of 51) and 7.8% (4 out of 51) of striatal minute-encoding neurons were identified as ramping-up and -down types, respectively (Figure 4E), consistent with the previous reports of ramping-up striatal firing patterns during decision making.[36,37] In addition, 33.3% (17 out of 51) of striatal minute-encoding neurons were identified as a specific peak firing type (Figure 4F; n = 12 neurons, $r = 0.34$, $p = 0.28$). No significant changes in average normalized modulation indexes of striatal minute-encoding neurons were observed during the 5-min interval (Figure 4G, bottom; $p > 0.05$, Tukey's test). Their SI was 4.06 (Figure S2H), which was significantly higher and lower than those of the shuffled datasets and the PS model, respectively, suggesting that their temporal tuning curves were structurally, but not perfectly, distributed across time, consistent with sequential activity of striatal neurons in the range of seconds reported from previous studies.[8,38,39] The average decoding error was significantly smaller than that of shuffled datasets (Figures 4I and S5C; n = 9 sessions from 5 rats, $t_8 = -2.93$, $p = 0.019$; paired t test). To test the contribution of hippocampal activity to the time encoding of striatal neurons, we recorded striatal neuronal spike patterns during inactivation of the dorsal hippocampus by muscimol (Figure 4J). In hippocampal muscimol-injected rats, the zTI_{spike} of active striatal neurons (0.1–10 Hz) was significantly lower than that in saline-injected rats (Figures 4J and S5E; $D_{max} = 0.38$, $p = 5.8 \times 10^{-4}$; Kolmogorov-Smirnov test). Decoding errors of time from hippocampal muscimol-injected rats were not significantly different from those of the corresponding shuffled datasets (Figures S5G and S5I; $t_3 = -1.19$, $p = 0.32$; paired t test; n = 4 sessions from 3 rats). Such effects were not observed in hippocampal saline-injected rats (Figures S5F and S5H; $t_5 = -4.50$, $p = 6.4 \times 10^{-3}$; paired t test; n = 6 sessions from 3 rats). These results suggest that striatal time encoding of minutes is sustained by hippocampal activity.

Experience-dependent minute encoding

We next asked whether such encoding of minutes is inherent in these neurons or whether it is first formed by learning the cognitive demands for time estimation. Four rats were habituated for several weeks to the task chamber with food presented at random time intervals (Figure S6A). On a recording day, they were subjected for the first time to the 5-min task condition, termed a novel 5-min task (Figure S6A). The rats did not exhibit apparent time-dependent increases in checking behavior throughout all trials in a session (Figures S6B and S6C). In the early phase of a session, neither hippocampal nor striatal neurons showed any apparent time-dependent spikes. Notably, some neurons started to show minute-encoding firing patterns in the later phase (Figures 5A and 5B). Such time-dependent changes were quantified by computing single-trial TI_{spike} every trial for each cell. Overall, as trials proceeded, the single-trial TI_{spike} values of all neurons (zTI_{spike} >1.04) significantly increased in both the hippocampus and striatum (Figures 5C and 5D, left; n = 19 hippocampal neurons, $F_{15,262} = 2.42$, $p = 2.7 \times 10^{-3}$; n = 13 striatal neurons, $F_{15,180} = 2.60$, $p = 1.5 \times 10^{-3}$; one-way ANOVA), and the percentage of neurons with prominent temporal changes in minutes in a trial (TI_{spike} >0.14) increased (Figures 5C and 5D, right). These results indicate that minute encoding in the hippocampal-striatal circuit first develops as animals initially learn repetitive changes in temporal contexts. Together with the observations that minute-encoding firing patterns already emerged in the later phase while animals did not exhibit apparent time-dependent changes in checking behavior (Figures S6B and S6C), these results suggest that (1) minute-encoding firing patterns are not perfectly correlated with the frequency of checking behavior and (2) the development of time-dependent spike signals in these brain regions can precede the expression of explicit behavior in such a novel condition.

We further analyzed the same spike patterns by a stepwise generalized linear model (GLM), similar to the analysis proposed by a previous study[30] (Figures S6D and S6E), to estimate whether temporal spike patterns are explained as linear functions of elapsed time in a trial (trial time), elapsed time over an entire period of a session (session time), checking behavior, and rat position. In the hippocampus and striatum, 22% (17 out 77) and 23% (6 out of 26) of neurons were selective for trial time (Figure S6D), respectively, consistent with the observations of neurons that developed encoding patterns for periods of minutes (Figures 5C and 5D). The percentage of hippocampal minute-encoding neurons appears to contradict a previous report by Tsao et al.[30] showing that only a small percentage of hippocampal CA3 cells encode trial time. These different results may have been due to the differences in experimental design: the rats in our study needed to be aware of the significance of time intervals every trial, while the rats used by Tsao et al.[30] were not specifically trained to attend the passage of time. Moreover, 26% (20 out 77) and 42% (11 out of 26) of active hippocampal and striatal neurons were selective for session time, respectively (Figure S6E), suggesting that the hippocampus and striatum continuously track the passage of time in longer timescales by recruiting time-drifting active neuronal ensembles, as previously observed.[20,24,25,30]

Scaling of minute encoding

We next asked whether the encoding of minutes by minute-encoding neurons has temporal scalability, as shown in second-range encoding.[8,40] In other words, the question is whether neurons encode specific time points in an absolute manner or flexibly scale their encoded time in response to changes in time intervals in a relative manner. In order to address this question, four rats were well trained in a task condition in which 5- and 8-min intervals with different light intensities (0.7 lux and 80 lux, respectively) alternated from trial to trial; this task was termed a 5/8-min task (Figure 6A). In each rat, raster plots and the percentage of checking behavior were separately computed for the two conditions (Figures 6B and 6C). If the rats could discriminate between the two conditions, the gradual increases in the frequency of checking behavior in the 8-min condition would be slower than those in the 5-min condition. This tendency was confirmed in all animals tested. Assuming that checking behavioral patterns

Please cite this article in press as: Shikano et al., Minute-encoding neurons in hippocampal-striatal circuits, Current Biology (2021), https://doi.org/10.1016/j.cub.2021.01.032

CellPress

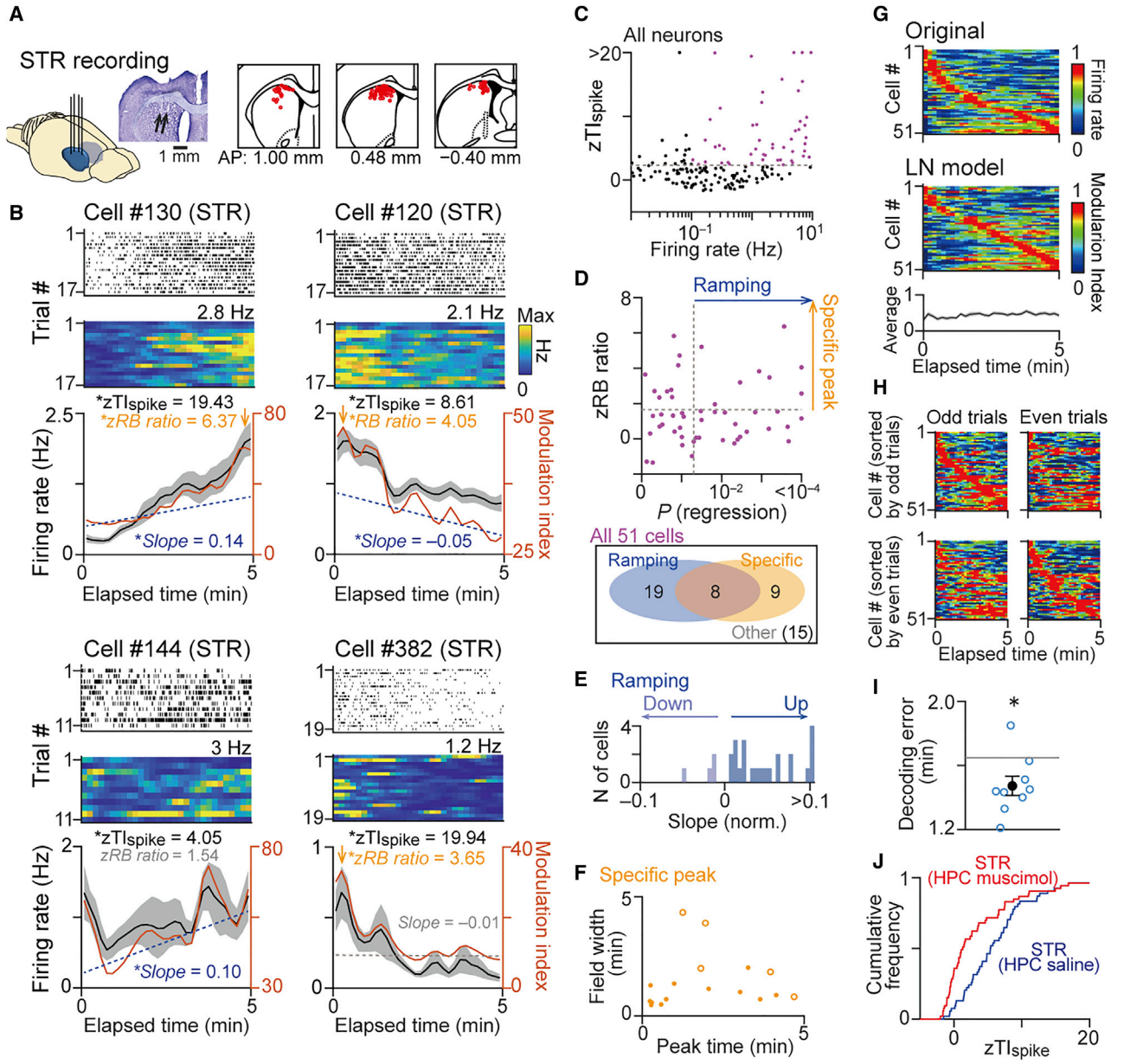

Figure 4. Minute encoding by striatal neurons

(A) (Left) Multiunit recordings were performed from the dorsal striatum (STR), as indicated by arrows on a coronal section. (Right) Superimpositions of recording sites for all 66 tetrodes from 13 rats, as indicated by red dots on coronal brain sections.

(B) Four representative minute-encoding neurons in the striatum, as shown in Figure 2C.

(C) Relationship between average firing rates and zTI_{spike} of all striatal neurons recorded (n = 185 neurons from 8 rats). Minute-encoding neurons are labeled in magenta (n = 51 neurons).

(D) Same as Figure 3B but for striatal minute-encoding neurons.

(E) Same as Figure 3C but for striatal minute-encoding neurons classified as a ramping firing type (n = 23 ramping-up and 4 ramping-down neurons).

(F) Same as Figure 3D but for striatal minute-encoding neurons classified as a specific peak firing type (n = 17 neurons).

(G) Original (top) and LN model-adjusted (middle) temporal tuning curves of all minute-encoding striatal neurons identified (zTI_{spike} >2.33), as shown in Figure 3E. (Bottom) Average changes in modulation indexes. $p > 0.05$ across time.

(H) Same as Figure 3F but for striatal minute-encoding neurons.

(I) Decoding errors (n = 9 sessions from 5 rats), as shown in Figure 3I. *$p < 0.05$; paired t test.

(J) Cumulative distributions of zTI_{spike} in rats injected with saline (blue, n = 54 neurons from 3 rats) and muscimol (red, n = 53 neurons from 3 rats) ($p < 0.001$; Kolmogorov-Smirnov test) into the hippocampus. See also Figures S2, S3, and S5.

Please cite this article in press as: Shikano et al., Minute-encoding neurons in hippocampal-striatal circuits, Current Biology (2021), https://doi.org/10.1016/j.cub.2021.01.032

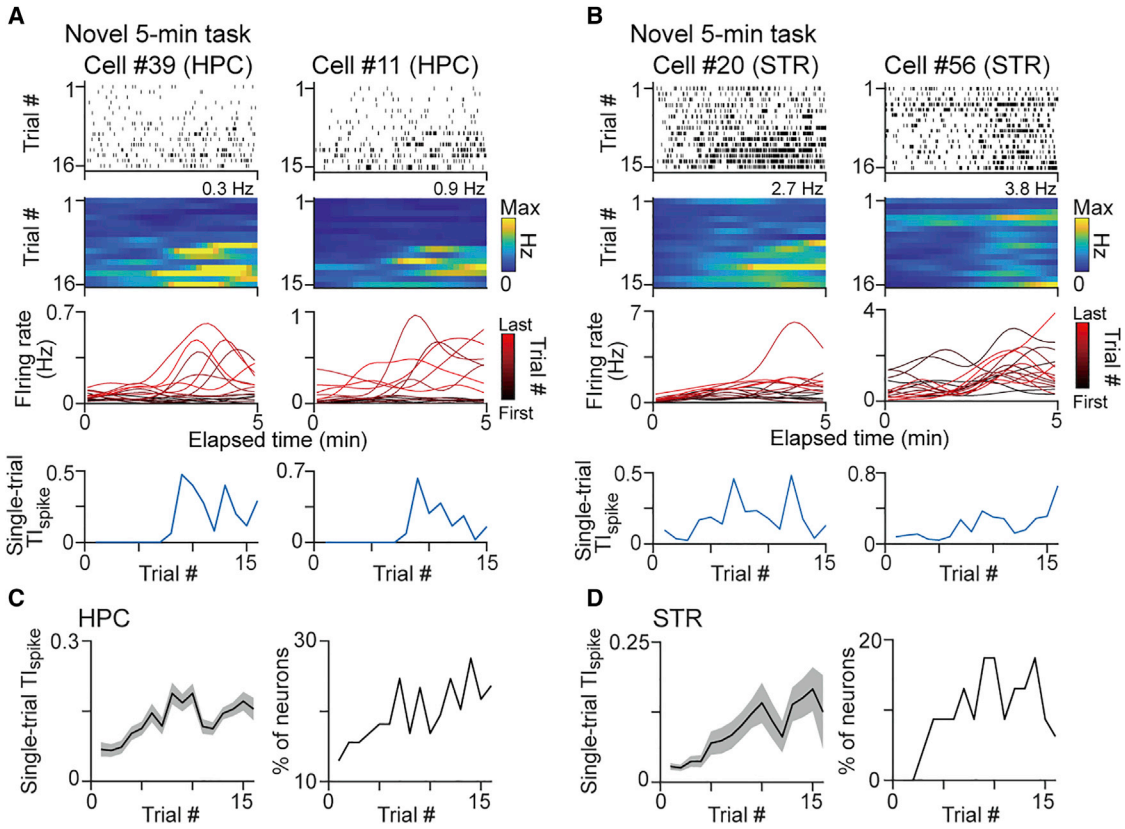

Figure 5. Minute encoding develops with learning

(A and B) Four representative minute-encoding neurons (A, HPC; B, STR) during a novel 5-min task. (From top to bottom) A raster plot showing spike patterns aligned to trial onset; the corresponding pseudocolor images show the instantaneous firing rates (bin = 10 s; blue and yellow represent zero and the peak firing rates described above), the same firing rates shown as temporal curves (each line represents each trial in a different color), and changes in single-trial TI_{spike}. (C) (Left) Changes in average single-trial TI_{spike} over all hippocampal cells tested (n = 19 neurons with a zTI_{spike} greater than 1.04 from 3 rats; $p < 0.001$, one-way ANOVA). (Right) The percentage of hippocampal neurons with single-trial TI_{spike} >0.14. The black line and gray regions represent the mean and SEM, respectively. (D) Same as (C) but for striatal neurons (n = 13 neurons from 2 rats; $p < 0.001$).
See also Figure S6.

were temporally scalable by a linear proportion, we defined the best scaling factor (best SF_{check}) that yielded the minimum difference between a scaled 5-min temporal curve and the 8-min curve. In the example session in Figure 6C, the best SF_{check} was computed to be 1.47, which was close to the value of 8/5 (the time-interval ratio between the 8- and 5-min conditions), suggesting that this rat could precisely adjust its gradual temporal increase in the checking behavior against the alternating time intervals. Here, the rats with the best SF_{check}, between 1.28 and 1.92 (less than a 20% difference from that of 8/5) (Figure 6D; n = 12 sessions), were considered to successfully discriminate the two time intervals and were used for subsequent spike analyses. For each neuron, as with checking behavior, the best scaling factor (best SF_{spike}) for spike-rate temporal tuning curves from two different conditions was computed (Figure 6E, bottom). In both the hippocampus and striatum, a subset of neurons with zTIspike more than 1.04 in both conditions (10/21 = 47.6% and 14/46 = 30.4%, respectively) had their best SF_{spike} between 1.28 and 1.92 (Figure 6F), suggesting that the encoding of minutes by hippocampal and striatal neurons is scalable in response to changes in external temporal contexts. On the other hand, the other subset of neurons had their best SF_{spike} at approximately 1, meaning that there is a small fraction of neurons showing scale-invariant encoding patterns (Figure 6F). To compare the trial-to-trial variability of spike patterns between the two conditions, we computed a coefficient of variation ($CV_{spike\ rate}$) of spike counts in individual trials. The distributions of $CV_{spike\ rate}$ did not significantly differ between the conditions (Figure 6G; HPC: n = 21 neurons, $D_{max} = 0.14$, p = 0.97; STR: n = 46 neurons, $D_{max} = 0.13$, p = 0.80), suggesting that the variability of spike counts to encode time does not prominently vary even when time ranges to be encoded were scaled.

DISCUSSION

In this study, we designed a behavioral task in which rats gradually increased reward-seeking (checking) behavior across repeated 5-min trials. To reduce the influences of behavioral factors such as moving space, speed, and exploratory behavior, the task chamber was minimized, and residual variations of these behavioral variables were statistically adjusted by the LN model. In these conditions, we identified hippocampal and striatal neuron populations encoding elapsed time on the order of minutes every

Please cite this article in press as: Shikano et al., Minute-encoding neurons in hippocampal-striatal circuits, Current Biology (2021), https://doi.org/10.1016/j.cub.2021.01.032

CellPress

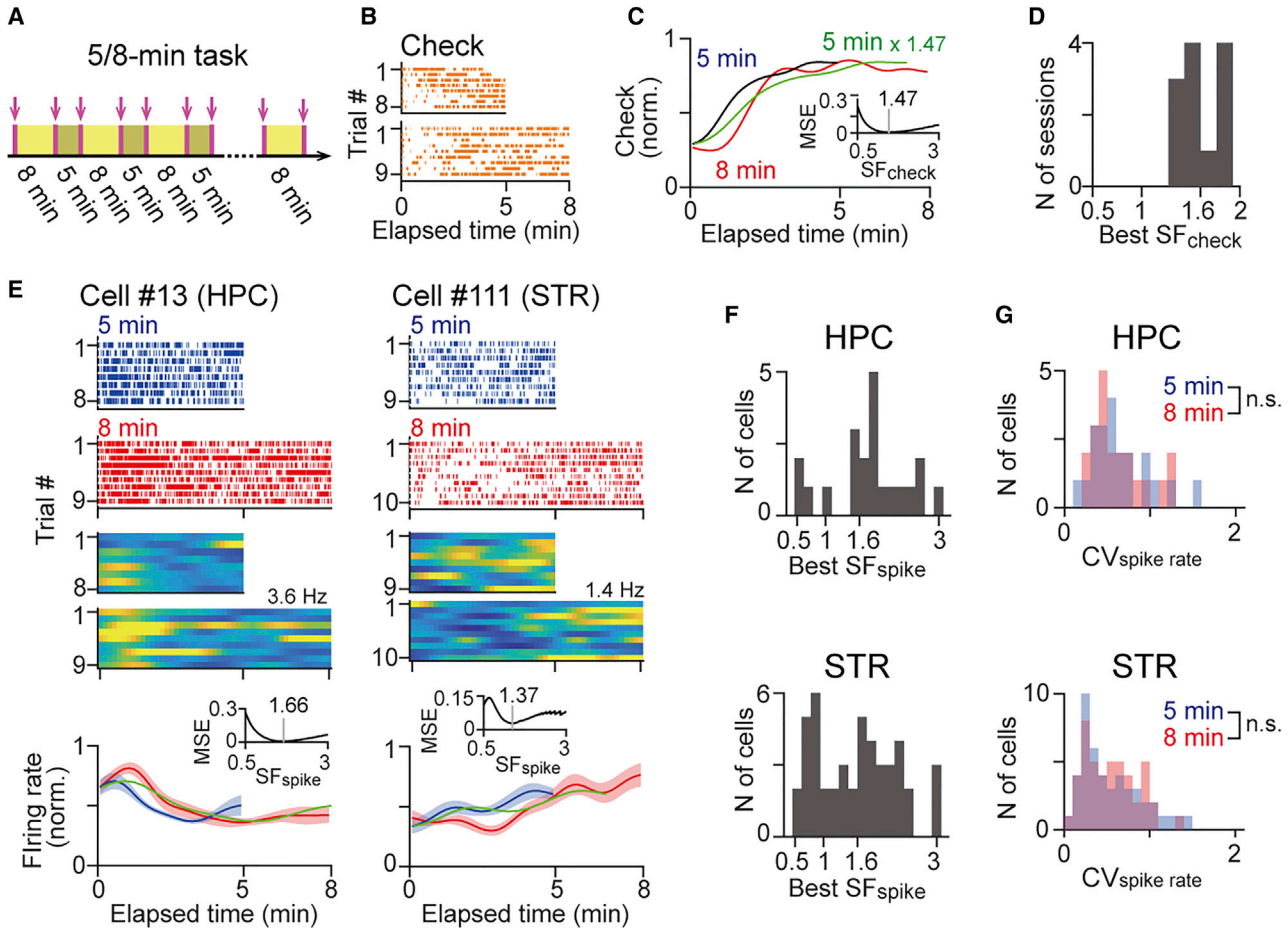

Figure 6. Rescaling of minute encoding

(A) Schematic of the 5/8-min task, where the intensity of light in the room was alternated between the 5- and 8-min conditions.

(B) Raster plots of checking behavior in a session plotted separately for the 5- and 8-min conditions.

(C) Average percentage of checking behavior computed from (B) (blue, 5 min; red, 8 min). The green line represents the 5-min condition expanded in time by a factor of 1.47, which was determined to be the best SF_{check}. (Inset) Relationship between SF_{check} and mean squared error (MSE) per time in the percentage of checking behavior between the 8-min trace and the expanded 5-min trace. The best SF_{check} was defined as the value that gave the minimum difference.

(D) Distribution of the best SF_{check} from all rats used for analysis (n = 12 sessions from 4 rats).

(E) Two representative neurons. (From top to bottom) Raster plot showing spike patterns plotted separately for the 5- and 8-min conditions; the corresponding pseudocolor images show the instantaneous firing rates (bin = 10 s; blue and yellow represent zero and the peak firing rates described beside the graph, respectively) and average temporal tuning curves in the 5- (blue) and 8-min (red) conditions. Thin regions represent SEM. The green line represents the tuning curve scaled by the best SF_{spike} (defined in the inset).

(F) Distributions of the best SF_{spike} of active hippocampal and striatal neurons (n = 21 and 46 neurons, respectively, from 3 rats).

(G) Comparisons of distributions of $CV_{spike\ rate}$ between the 5- (blue) and 8-min (red) conditions (n = 21 and 46 neurons, respectively, from 3 rats).

trial. We note that some neurons showed a substantial correlation between minute-encoding firing patterns and the frequency of checking behavior, but this correlation alone did not explain temporal changes in their firing patterns in the range of minutes. Such time coding did not emerge in rats when they first encountered the task condition, but it gradually developed as the rats repeatedly experienced the time-reward relationships. The learning-dependent changes in checking behavior and neuronal activity confirm that it is highly unlikely that the temporal changes observed in our task are simply determined by constant sensory and enterogastric signals. The temporal profiles could be flexibly expanded and compressed in time in response to changes in the time interval until reward presentation.

While accumulating evidence demonstrates the importance of the hippocampus and striatum in temporal information processing on the order of seconds, as typically represented by hippocampal time cells[12,13,15,41] and striatal ramping cells,[8,9,11] there is little evidence of neurophysiological mechanisms for temporal processing at a timescale greater than seconds. This is because it has been difficult to establish behavioral tasks where rodents can recognize temporal contexts with such long durations while securing sufficient numbers of trials to verify data reproducibility. A previous study[21] circumvented this issue by repeatedly training rats to discriminate different elapsed times on a timescale of minutes to efficiently obtain rewards baited at different locations depending on the time length. This study

Please cite this article in press as: Shikano et al., Minute-encoding neurons in hippocampal-striatal circuits, Current Biology (2021), https://doi.org/10.1016/j.cub.2021.01.032

demonstrated the necessity of the hippocampus to process temporal information on a timescale of minutes at a behavioral level. Consistent with this study, our behavioral task was also hippocampus dependent and, furthermore, specialized to test reproducible neuronal activity that changed over minutes.

Minute-encoding neurons found in this study appear analogous to cells that encode seconds observed from previous studies: (1) each neuron encodes discrete time periods,[13,15] (2) their time fields cover an entire time period, as represented by the sequential emergence of the time fields, (3) their time fields become broader the later they appear, and (4) their time fields develop as animals gain experience with the task,[14] and (5) their time fields are scalable, correlated with animal's timing behavior.[8,40] These common features of time fields suggest that the roles of second-encoding cells and minute-encoding cells might be similar in bridging temporal gaps among discontiguous key events at different timescales. Our results did not mean the perfect sequential patterns of minute-encoding neuronal firing in the 5-min time interval. Nonetheless, considering the observations of neurons of both ramping-up and ramping-down firing types that could potentially encode the start and end points of a time interval, respectively, and neurons encoding specific time periods within a brief window between these two time points, our results suggest that the combination of these diverse firing properties might be an efficient strategy for neuronal populations to cover minute-range time periods without missing encoding of specific time points.

Entorhinal cortical neurons have been shown to exhibit temporally decaying firing patterns in response to a stimulus and contexts in the range of seconds[42] and minutes,[30] which have been suggested as neural substrates of leaky integrators encoding the Laplace transform of input patterns at a variety of rates.[43] Such slowly decaying spike patterns produced by entorhinal cortical neurons may serve as a primary driver for sequential activation of hippocampal time-encoding neurons[44] both in the range of seconds[12,13] and minutes as observed in our study. In addition, especially for our task including varying behavior in reference to the time of reward presentations, reward-prediction-related dopaminergic signals[45,46] are potentially linked to the minute-range encoding. This idea is supported by anatomical observations that the hippocampus[47–49] and striatum[50] receive dopaminergic projections from the midbrain or locus coeruleus. Consistently, the nigrostriatal dopaminergic pathway has been shown to modulate temporal judgment in the range of seconds.[50]

The partial reduction in minute-encoding cells in the striatum by hippocampal inactivation suggests that temporal information is functionally processed in the hippocampal-striatal circuits. Considering the anatomical observation that dorsal hippocampal CA1 neurons send a minor direct projection to the striatum, the functional associations may be explained by indirect polysynaptic routes through the other brain areas. Among them, the medial prefrontal cortex may play a key role in this interregional interaction as it has been shown to process temporal signals,[40,51] especially when dopaminergic signals are provided. Together with the fact that the hippocampus and the prefrontal cortex are bidirectionally connected[52–56] and the prefrontal cortex controls temporal processing of the striatum,[35] a functional interaction in the hippocampal-prefrontal circuits may be a primary determinant of minute-range encoding in the striatum. Future studies are needed to clarify whether minute-encoding neurons are distributed in timing systems outside the hippocampal-striatal circuits.[5]

We demonstrated that the temporal tuning of minute-encoding neurons is flexibly organized in response to novel experiences and external environmental changes. These results suggest that minute-encoding neurons measure elapsed time from a specific temporal landmark in a relative rather than absolute manner and that they maintain temporal continuity at a timescale of minutes. Our demonstration of the encoding of minutes adds to a series of studies of neuronal mechanisms underlying time encoding at shorter and longer timescales, such as second-range time cells,[12,13,15,41] and systematically varying active neuron ensembles over hours and days,[24,27,30] and suggests the capacity of hippocampal and striatal neurons to multiplex temporal information at diverse timescales.

STAR★METHODS

Detailed methods are provided in the online version of this paper and include the following:

- KEY RESOURCES TABLE
- RESOURCE AVAILABILITY
  - Lead contact
  - Materials availability
  - Data and code availability
- EXPERIMENTAL MODEL AND SUBJECT DETAILS
- METHOD DETAILS
  - Five-minute task
  - Novel 5-min task
  - Five/eight-minute task
  - Surgical procedures
  - Adjusting electrode depth
  - Electrophysiological recording
  - Muscimol injection
  - Random foraging task
  - Histological analysis to confirm electrode placement or cannula placement
- QUANTIFICATION AND STATISTICAL ANALYSIS
  - Spike sorting
  - Analysis of behavioral patterns
  - Analysis of temporal spike patterns
  - Trial-to-trial variability of spike counts in time-encoding neurons
  - Bayesian decoding of elapsed time
  - Scaling factor for the 5/8-min task
  - GLM fitting throughout a recording session
  - Statistical analysis

SUPPLEMENTAL INFORMATION

Supplemental Information can be found online at https://doi.org/10.1016/j.cub.2021.01.032.

ACKNOWLEDGMENTS

This work was supported by KAKENHI (19H04897, 17H05939, and 20H03545) from the Japan Society for the Promotion of Science(JSPS), a Precursory Research for Embryonic Science and Technology grant (JPMJPR1785) from

the Japan Science and Technology Agency (JST), and a grant from the Advanced Research and Development Programs for Medical Innovation (1041630) of the Japan Agency for Medical Research and Developmen-t(AMED) to T.S.; funds from the JST Exploratory Research for Advanced Technology (JPMJER1801) and the AMED Strategic International Brain Science Research Promotion Program (18dm0307007h0001) to Y.I.; and a JSPS Research Fellowship for Young Scientists to Y.S. We would like to acknowledge Christopher J. MacDonald for providing us with the original spike data of time cells published by MacDonald et al.[13]

AUTHOR CONTRIBUTIONS

Y.S. and T.S. designed the study. Y.S. performed the surgery, acquired the electrophysiological data, and performed the analysis. Y.I. supervised the project. Y.S. and T.S. prepared all the figures. Y.S. and T.S. wrote the main manuscript text, and all authors reviewed the main manuscript text.

DECLARATION OF INTERESTS

The authors declare no competing interests.

Received: August 23, 2020
Revised: November 16, 2020
Accepted: January 11, 2021
Published: February 4, 2021

REFERENCES

1. Richards, W. (1973). Time reproductions by H.M. Acta Psychol. (Amst.) *37*, 279–282.
2. Olton, D.S., Meck, W.H., and Church, R.M. (1987). Separation of hippocampal and amygdaloid involvement in temporal memory dysfunctions. Brain Res. *404*, 180–188.
3. Meck, W.H., Church, R.M., Wenk, G.L., and Olton, D.S. (1987). Nucleus basalis magnocellularis and medial septal area lesions differentially impair temporal memory. J. Neurosci. *7*, 3505–3511.
4. Malapani, C., Rakitin, B., Levy, R., Meck, W.H., Deweer, B., Dubois, B., and Gibbon, J. (1998). Coupled temporal memories in Parkinson's disease: a dopamine-related dysfunction. J. Cogn. Neurosci. *10*, 316–331.
5. Buhusi, C.V., and Meck, W.H. (2005). What makes us tick? Functional and neural mechanisms of interval timing. Nat. Rev. Neurosci. *6*, 755–765.
6. Meck, W.H. (2006). Neuroanatomical localization of an internal clock: a functional link between mesolimbic, nigrostriatal, and mesocortical dopaminergic systems. Brain Res. *1109*, 93–107.
7. Yin, B., and Meck, W.H. (2014). Comparison of interval timing behaviour in mice following dorsal or ventral hippocampal lesions with mice having δ-opioid receptor gene deletion. Philos. Trans. R. Soc. Lond. B Biol. Sci. *369*, 20120466.
8. Mello, G.B., Soares, S., and Paton, J.J. (2015). A scalable population code for time in the striatum. Curr. Biol. *25*, 1113–1122.
9. Bakhurin, K.I., Goudar, V., Shobe, J.L., Claar, L.D., Buonomano, D.V., and Masmanidis, S.C. (2017). Differential Encoding of Time by Prefrontal and Striatal Network Dynamics. J. Neurosci. *37*, 854–870.
10. Matell, M.S., and Meck, W.H. (1999). Reinforcement-induced within-trial resetting of an internal clock. Behav. Processes *45*, 159–171.
11. Matell, M.S., Meck, W.H., and Nicolelis, M.A. (2003). Interval timing and the encoding of signal duration by ensembles of cortical and striatal neurons. Behav. Neurosci. *117*, 760–773.
12. Pastalkova, E., Itskov, V., Amarasingham, A., and Buzsáki, G. (2008). Internally generated cell assembly sequences in the rat hippocampus. Science *321*, 1322–1327.
13. MacDonald, C.J., Lepage, K.Q., Eden, U.T., and Eichenbaum, H. (2011). Hippocampal "time cells" bridge the gap in memory for discontiguous events. Neuron *71*, 737–749.
14. Gill, P.R., Mizumori, S.J., and Smith, D.M. (2011). Hippocampal episode fields develop with learning. Hippocampus *21*, 1240–1249.
15. Kraus, B.J., Robinson, R.J., 2nd, White, J.A., Eichenbaum, H., and Hasselmo, M.E. (2013). Hippocampal "time cells": time versus path integration. Neuron *78*, 1090–1101.
16. MacDonald, C.J., Carrow, S., Place, R., and Eichenbaum, H. (2013). Distinct hippocampal time cell sequences represent odor memories in immobilized rats. J. Neurosci. *33*, 14607–14616.
17. Kraus, B.J., Brandon, M.P., Robinson, R.J., 2nd, Connerney, M.A., Hasselmo, M.E., and Eichenbaum, H. (2015). During Running in Place, Grid Cells Integrate Elapsed Time and Distance Run. Neuron *88*, 578–589.
18. Nakazono, T., Sano, T., Takahashi, S., and Sakurai, Y. (2015). Theta oscillation and neuronal activity in rat hippocampus are involved in temporal discrimination of time in seconds. Front. Syst. Neurosci. *9*, 95.
19. Salz, D.M., Tiganj, Z., Khasnabish, S., Kohley, A., Sheehan, D., Howard, M.W., and Eichenbaum, H. (2016). Time Cells in Hippocampal Area CA3. J. Neurosci. *36*, 7476–7484.
20. Mau, W., Sullivan, D.W., Kinsky, N.R., Hasselmo, M.E., Howard, M.W., and Eichenbaum, H. (2018). The Same Hippocampal CA1 Population Simultaneously Codes Temporal Information over Multiple Timescales. Curr. Biol. *28*, 1499–1508.
21. Jacobs, N.S., Allen, T.A., Nguyen, N., and Fortin, N.J. (2013). Critical role of the hippocampus in memory for elapsed time. J. Neurosci. *33*, 13888–13893.
22. MacDonald, C.J., and Meck, W.H. (2005). Differential effects of clozapine and haloperidol on interval timing in the supraseconds range. Psychopharmacology (Berl.) *182*, 232–244.
23. Mankin, E.A., Diehl, G.W., Sparks, F.T., Leutgeb, S., and Leutgeb, J.K. (2015). Hippocampal CA2 activity patterns change over time to a larger extent than between spatial contexts. Neuron *85*, 190–201.
24. Mankin, E.A., Sparks, F.T., Slayyeh, B., Sutherland, R.J., Leutgeb, S., and Leutgeb, J.K. (2012). Neuronal code for extended time in the hippocampus. Proc. Natl. Acad. Sci. USA *109*, 19462–19467.
25. Ziv, Y., Burns, L.D., Cocker, E.D., Hamel, E.O., Ghosh, K.K., Kitch, L.J., El Gamal, A., and Schnitzer, M.J. (2013). Long-term dynamics of CA1 hippocampal place codes. Nat. Neurosci. *16*, 264–266.
26. Rubin, A., Geva, N., Sheintuch, L., and Ziv, Y. (2015). Hippocampal ensemble dynamics timestamp events in long-term memory. eLife *4*, e12247.
27. Manns, J.R., Howard, M.W., and Eichenbaum, H. (2007). Gradual changes in hippocampal activity support remembering the order of events. Neuron *56*, 530–540.
28. Naya, Y., and Suzuki, W.A. (2011). Integrating what and when across the primate medial temporal lobe. Science *333*, 773–776.
29. Hardcastle, K., Maheswaranathan, N., Ganguli, S., and Giocomo, L.M. (2017). A Multiplexed, Heterogeneous, and Adaptive Code for Navigation in Medial Entorhinal Cortex. Neuron *94*, 375–387.
30. Tsao, A., Sugar, J., Lu, L., Wang, C., Knierim, J.J., Moser, M.B., and Moser, E.I. (2018). Integrating time from experience in the lateral entorhinal cortex. Nature *561*, 57–62.
31. Orhan, A.E., and Ma, W.J. (2019). A diverse range of factors affect the nature of neural representations underlying short-term memory. Nat. Neurosci. *22*, 275–283.
32. Harvey, C.D., Coen, P., and Tank, D.W. (2012). Choice-specific sequences in parietal cortex during a virtual-navigation decision task. Nature *484*, 62–68.
33. Pastalkova, E., Wang, Y., Mizuseki, K., and Buzsáki, G. (2015). Simultaneous extracellular recordings from left and right hippocampal areas CA1 and right entorhinal cortex from a rat performing a left / right alternation task and other behaviors. hc-5 (CRCNS data sharing website).
34. Emmons, E.B., Ruggiero, R.N., Kelley, R.M., Parker, K.L., and Narayanan, N.S. (2016). Corticostriatal Field Potentials Are Modulated at Delta and Theta Frequencies during Interval-Timing Task in Rodents. Front. Psychol. *7*, 459.

35. Emmons, E.B., De Corte, B.J., Kim, Y., Parker, K.L., Matell, M.S., and Narayanan, N.S. (2017). Rodent Medial Frontal Control of Temporal Processing in the Dorsomedial Striatum. J. Neurosci. *37*, 8718–8733.

36. van der Meer, M.A., Johnson, A., Schmitzer-Torbert, N.C., and Redish, A.D. (2010). Triple dissociation of information processing in dorsal striatum, ventral striatum, and hippocampus on a learned spatial decision task. Neuron *67*, 25–32.

37. van der Meer, M.A., and Redish, A.D. (2011). Theta phase precession in rat ventral striatum links place and reward information. J. Neurosci. *31*, 2843–2854.

38. Akhlaghpour, H., Wiskerke, J., Choi, J.Y., Taliaferro, J.P., Au, J., and Witten, I.B. (2016). Dissociated sequential activity and stimulus encoding in the dorsomedial striatum during spatial working memory. eLife *5*, e19507.

39. Adler, A., Katabi, S., Finkes, I., Israel, Z., Prut, Y., and Bergman, H. (2012). Temporal convergence of dynamic cell assemblies in the striato-pallidal network. J. Neurosci. *32*, 2473–2484.

40. Xu, M., Zhang, S.Y., Dan, Y., and Poo, M.M. (2014). Representation of interval timing by temporally scalable firing patterns in rat prefrontal cortex. Proc. Natl. Acad. Sci. USA *111*, 480–485.

41. Robinson, N.T.M., Priestley, J.B., Rueckemann, J.W., Garcia, A.D., Smeglin, V.A., Marino, F.A., and Eichenbaum, H. (2017). Medial Entorhinal Cortex Selectively Supports Temporal Coding by Hippocampal Neurons. Neuron *94*, 677–688.

42. Bright, I.M., Meister, M.L.R., Cruzado, N.A., Tiganj, Z., Buffalo, E.A., and Howard, M.W. (2020). A temporal record of the past with a spectrum of time constants in the monkey entorhinal cortex. Proc. Natl. Acad. Sci. USA *117*, 20274–20283.

43. Howard, M.W., MacDonald, C.J., Tiganj, Z., Shankar, K.H., Du, Q., Hasselmo, M.E., and Eichenbaum, H. (2014). A unified mathematical framework for coding time, space, and sequences in the hippocampal region. J. Neurosci. *34*, 4692–4707.

44. Rolls, E.T., and Mills, P. (2019). The Generation of Time in the Hippocampal Memory System. Cell Rep. *28*, 1649–1658.

45. Howe, M.W., Tierney, P.L., Sandberg, S.G., Phillips, P.E., and Graybiel, A.M. (2013). Prolonged dopamine signalling in striatum signals proximity and value of distant rewards. Nature *500*, 575–579.

46. Schultz, W., Dayan, P., and Montague, P.R. (1997). A neural substrate of prediction and reward. Science *275*, 1593–1599.

47. Takeuchi, T., Duszkiewicz, A.J., Sonneborn, A., Spooner, P.A., Yamasaki, M., Watanabe, M., Smith, C.C., Fernández, G., Deisseroth, K., Greene, R.W., and Morris, R.G. (2016). Locus coeruleus and dopaminergic consolidation of everyday memory. Nature *537*, 357–362.

48. Kempadoo, K.A., Mosharov, E.V., Choi, S.J., Sulzer, D., and Kandel, E.R. (2016). Dopamine release from the locus coeruleus to the dorsal hippocampus promotes spatial learning and memory. Proc. Natl. Acad. Sci. USA *113*, 14835–14840.

49. Wagatsuma, A., Okuyama, T., Sun, C., Smith, L.M., Abe, K., and Tonegawa, S. (2018). Locus coeruleus input to hippocampal CA3 drives single-trial learning of a novel context. Proc. Natl. Acad. Sci. USA *115*, E310–E316.

50. Soares, S., Atallah, B.V., and Paton, J.J. (2016). Midbrain dopamine neurons control judgment of time. Science *354*, 1273–1277.

51. Narayanan, N.S., Land, B.B., Solder, J.E., Deisseroth, K., and DiLeone, R.J. (2012). Prefrontal D1 dopamine signaling is required for temporal control. Proc. Natl. Acad. Sci. USA *109*, 20726–20731.

52. van Groen, T., and Wyss, J.M. (1990). Extrinsic projections from area CA1 of the rat hippocampus: olfactory, cortical, subcortical, and bilateral hippocampal formation projections. J. Comp. Neurol. *302*, 515–528.

53. Swanson, L.W. (1981). A direct projection from Ammon's horn to prefrontal cortex in the rat. Brain Res. *217*, 150–154.

54. Ferino, F., Thierry, A.M., and Glowinski, J. (1987). Anatomical and electrophysiological evidence for a direct projection from Ammon's horn to the medial prefrontal cortex in the rat. Exp. Brain Res. *65*, 421–426.

55. Cenquizca, L.A., and Swanson, L.W. (2007). Spatial organization of direct hippocampal field CA1 axonal projections to the rest of the cerebral cortex. Brain Res. Brain Res. Rev. *56*, 1–26.

56. Gabbott, P.L.A., Warner, T.A., Jays, P.R.L., Salway, P., and Busby, S.J. (2005). Prefrontal cortex in the rat: projections to subcortical autonomic, motor, and limbic centers. J. Comp. Neurol. *492*, 145–177.

57. Shikano, Y., Sasaki, T., and Ikegaya, Y. (2018). Simultaneous Recordings of Cortical Local Field Potentials, Electrocardiogram, Electromyogram, and Breathing Rhythm from a Freely Moving Rat. J. Vis. Exp. *134*, 56980.

58. Redish, A.D. (2009). MClust 3.5, Free-Ware Spike Sorting (University of Minnesota), Available at http://redishlab.neuroscience.umn.edu/MClust/MClust.html.

59. Schmitzer-Torbert, N., Jackson, J., Henze, D., Harris, K., and Redish, A.D. (2005). Quantitative measures of cluster quality for use in extracellular recordings. Neuroscience *131*, 1–11.

Please cite this article in press as: Shikano et al., Minute-encoding neurons in hippocampal-striatal circuits, Current Biology (2021), https://doi.org/10.1016/j.cub.2021.01.032

CellPress

STAR★METHODS

KEY RESOURCES TABLE

REAGENT or RESOURCE	SOURCE	IDENTIFIER
Chemicals, peptides, and recombinant proteins		
Muscimol	Sigma-Aldrich	M1523-10MG
Deposited data		
Behavior and spike data	Mendeley Data	https://dx.doi.org/10.17632/b4j6nbkj3d.1
Experimental models: organisms/strains		
Long Evans rats	Japan SLC	Iar: Long-Evans
Software and algorithms		
MATLAB R2018b	MathWorks	https://www.mathworks.com/products/matlab.html?s_tid=hp_products_matlab
MClust	By A. David Redish	http://redishlab.neuroscience.umn.edu/MClust/MClust.html
CerePlex Direct Software Suite	Blackrock Microsystems	https://www.blackrockmicro.com/technical-support/software-downloads/

RESOURCE AVAILABILITY

Lead contact

Further information and requests for resources and reagents should be directed to and will be fulfilled by the Lead Contact, Takuya Sasaki (tsasaki@mol.f.u-tokyo.ac.jp).

Materials availability

This study did not generate any unique reagents. The CAD files for creating the feeding wheel and feeding port by 3D printers are available from the lead contact upon request.

Data and code availability

The original data are provided on Mendeley Data (https://dx.doi.org/10.17632/b4j6nbkj3d.1). The codes are available from the lead contact upon request.

EXPERIMENTAL MODEL AND SUBJECT DETAILS

All experiments were performed with the approval of the Experimental Ethics Committee at the University of Tokyo (approval number: P29-11) and according to the NIH guidelines for the care and use of rats.

All rats were purchased from SLC (Shizuoka, Japan). The rats were housed individually and maintained on a 12-h light/12-h dark schedule with lights off at 7:00 AM. All behavioral experiments occurred in the dark phase. Following at least 1 week of adaptation to the laboratory, the rats were housed individually and reduced to 85% of their *ad libitum* weight through limited daily feeding. Water was readily available.

A total of 24 male Long Evans rats (3–10 months old) with preoperative weights of 300–400 g were used in this study. The rats were housed individually and maintained on a 12-h light/12-h dark schedule with the lights turned off at 7:00 AM. All rats were purchased from SLC (Shizuoka, Japan). Following at least 1 week of laboratory adaptation, the rats were reduced to 85% of their *ad libitum* weight by limiting daily feeding. Water was readily available.

METHOD DETAILS

Five-minute task

Twelve rats performed a 5-min task in a 25-cm-sided square recording box (elevated 75 cm from the floor) with a wall height of 60 cm (Figure S1A). All behavioral experiments occurred in the dark phase with a light intensity of 0.7 lux. A feeding port (length = 8.9 cm,

Please cite this article in press as: Shikano et al., Minute-encoding neurons in hippocampal-striatal circuits, Current Biology (2021), https://doi.org/10.1016/j.cub.2021.01.032

height = 1.3 cm) with a pellet-presenting circular well (diameter = 9 mm) made of PLA resin created by a 3D printer (UP Plus2, Tiertime, Beijing, China) was attached to a corner of the box (Figures 1A and S1A). The size of the recording box was selected to obtain effective behavior without apparent stressful responses (e.g., jumping and biting) in the task, which could not be obtained with smaller sizes. An infrared photoreflector (LBR-127HLD, Letex Technology Corp., Taichung Hsien, Taiwan) was attached to the wall 13 mm beside the port to detect rats' checking behavior at the port. Periods during which rats were detected by the checking sensor were considered checking behavior. In the task, the port dispensed a 45-mg food pellet (Precision Pellets, F0021-J, Bioserv, Flemington, NJ) in the well for 3 s every 5 min, which was automatically regulated by a custom-made rotating feeding wheel including holes along the edge to accommodate a pellet (for a detailed image, see Figure S1A). The feeding wheel quickly (less than 1 s) rotated clockwise 5 min after a prior food dispensation event, which was controlled by a microcomputer board (Arduino UNO, Arduino S.R.L., Italy), and a hole that moved into the box dispensed a pellet to the rat. Pellet dispensation made a small ticking sound, serving as a cue signal for pellet presentation. In addition, during the 3 s pellet presentation periods, an inward-facing green light-emitting diode (LED) attached to the wall 7 cm beside the port was continuously illuminated as a cue signal. Because the food supply and cue presentation were controlled by a microcomputer board, it was not necessary to handle the rats and the apparatus once a task began. If the pellets were not consumed during the 3 s presentation periods, the pellets were automatically removed by quickly rotating the wheel so that the rats could no longer access them. Pellet removal also made a small ticking sound, similar to pellet dispensation, serving as a cue signal. A task session consisted of 20 pellet presentations and 5 or fewer omissions in which neither pellet nor any cues were presented for 5 min until the next presentation, resulting in one session lasting for 100–125 min. Omission events did not occur successively. Omission events were not included in training periods and were first included when the rats completed training (as described later) and the task sessions with electrophysiological recordings started. A trial was counted as a period from a time point when a rat could correctly consume a pellet during a 3 s presentation period to a time point when the next food presentation occurred after 5 min; consumption of the pellet signified a success event. A success trial was defined as a trial in which the rats could consume food within a 3 s pellet presentation period after waiting for 5 min, whereas a miss trial was defined as a trial in which a rat did not consume food within the 3 s pellet presentation period. An omission trial was defined as a trial in which an omission event occurred after 5 min of waiting. In the recording box, no apparent signs of pain or discomfort were observed.

To monitor the moment-to-moment position of the rats, an infrared video camera (MCM-303NIR-880-LED, Gazo Co., Ltd., Niigata, Japan; 0.37 cm/pixel) was attached to the ceiling, and three 1.5 × 2.0 cm rectangular-shaped infrared reflective tapes were attached to the electrode assembly on the rat's head in an isosceles triangle shape (base = 4 cm, legs = 6.8 cm) with the vertex oriented opposite to the rat's head direction. Reflection sites were tracked at 15 Hz using the camera. A head direction and a position at each frame were computed offline from the three reflection sites by a custom-made MATLAB program. The rats were kept in a rest box (20 × 20 cm) outside the field for tens of minutes before and after the task.

Before surgery, the rats were trained to learn the 5-min task. In all training periods, omission events were not included. On the first 2 days, the rats were subjected to a single session (100 min) of the 5-min task. On the third day, the rat was subjected to the same task condition, and an experimenter gently moved the rat so that it recognized the presentation of food at the reward port. After these three days of habituation, the rats were trained to perform a single session (100 min) of the 5-min task without omission events. This training was repeated daily until the rats learned the task and were able to consume food pellets 19–20 times out of 20 pellet presentations (95%–100% correct probability) for three consecutive days. To achieve this criterion performance, training lasted for 18–43 days. The rats that met the criteria were termed well-trained rats.

Novel 5-min task

Four rats were first habituated to the task chamber and the feeding port for at least 7 days. During each habituation process, 20 food pellets were presented for 3 s at random intervals of 4–20 s (Figure S6A). During the food presentation time, the cue light was turned on. Habituation was terminated if the rats successfully consumed 95%–100% of pellets in three successive habituation processes. On a recording day, the rats were subjected to the 5-min task for the first time, termed a novel 5-min task. For each rat, the first session including successful consumption of more than 16 pellets was analyzed as a novel 5-min task session.

Five/eight-minute task

Four rats were trained to perform an alternation between a 5-min task and an 8-min task in each trial, termed a 5/8-min task (Figure 6A). The 5/8-min task had no omission trials in either the training phases or recording periods. The rats were first trained for an 8-min task alone, which was similar to the 5-min task except that the waiting interval was 8 min and room lights were turned on with a light intensity of 80 lux so that the rats could differentiate the 8-min condition from the 5-min condition. The 8-min task included 20 trials (160 min), and training was repeated daily until the rats learned the task and were able to consume food pellets 19–20 times out of 20 pellet presentations (95%–100% correct probability) for three consecutive days. To achieve this performance criterion, training lasted for 20–25 days. The rats were then trained for the 5-min task alone, as described above. The 5-min task included 20 trials (100 min), and training was repeated daily until the rats learned the task and were able to consume food pellets 19–20 times out of 20 pellet presentations (95%–100% correct probability) for three consecutive days. To achieve this criterion performance, training lasted for 8–10 days. Last, the rats were trained for a task in which the 5-min and 8-min conditions alternated every trial, termed a 5/8-min task. A session of the 5/8-min task always started with the 8-min condition and consisted of a total of 10 trials

Please cite this article in press as: Shikano et al., Minute-encoding neurons in hippocampal-striatal circuits, Current Biology (2021), https://doi.org/10.1016/j.cub.2021.01.032

with the 8-min condition and 9 trials with the 5-min condition, resulting in a total time of 125 min. At each training stage, the rats were trained until they successfully consumed 95%–100% of pellets for 3 successive sessions. To achieve this performance criterion, training lasted for 8–10 days.

Surgical procedures

Twenty-three rats underwent surgery for implanting electrodes, as described elsewhere[57]. Briefly, the rat was anesthetized with isoflurane gas (1%–2.5%), and a 2-cm-long midline incision was made from the area between the eyes to the cerebellum. Craniotomies with a diameter of up to 3 mm were created above the right hippocampus (3.8 mm posterior and 2.5 mm lateral to the bregma) and the dorsal striatum (0.5 mm anterior and 2.5 mm lateral to the bregma) using a high-speed drill, and the dura was surgically removed. Two stainless-steel screws were implanted on the skull above the cerebellum to serve as ground electrodes. An electrode assembly that consisted of 16 independently movable tetrodes, which was created using a 3D printer (Form 2, Formlabs, Somerville, MA), was split into two sets of 8 tetrode bundles with an interval of 4.3 mm and stereotaxically implanted above the two craniotomies. The tips of the tetrode bundles were lowered to the cortical surface, and the electrodes were inserted 1.25 mm into the brain at the end of surgery. The electrodes were constructed from 17-μm-wide polyimide-coated platinum-iridium (90/10%) wire (California Fine Wire California Fine Wire Co., Grover Beach, CA), and the electrode tips were plated with platinum to lower the impedance of the electrodes to 150–300 kΩ at 1 kHz.

For injection of muscimol into the hippocampus, four rats underwent surgery during which a guide cannula (outer diameter = 0.5 mm) was implanted. Two craniotomies with a diameter of up to 0.9 mm were created at coordinates of 5.6 mm posterior and 2.5 mm bilateral to the bregma. For each craniotomy, a guide cannula was implanted with a depth of 3.7 mm and was inserted into the tissue at an angle of 30° in the coronal plane into the dorsal hippocampus. To prevent drying in the guide cannula, a dummy plastic cannula with a diameter of 0.37 mm was inserted into the guide tube.

All the recording devices and the cannula were secured to the skull using stainless-steel screws and dental cement. Following surgery, each rat was housed individually in transparent Plexiglass with free access to water and food for at least 3 days and was then food deprived to 85% of their body weight. Behavioral training and electrophysiological recordings commenced more than one week after the surgery.

Adjusting electrode depth

Each rat was connected to the recording equipment via CerePlex M (Blackrock Microsystems, Salt Lake City, UT), a digitally programmable amplifier, close to the rat's head. The output of the headstage was transmitted via a lightweight multiwire tether and a commutator to the CerePlex Direct recording system (Blackrock Microsystems), a data acquisition system. Electrode turning was performed while the rat was resting in a rest box. Electrode tips were advanced slowly, 30–250 μm per day, for 21–28 days until spiking cells were encountered in the CA1 layer of the hippocampus and the dorsal striatum, which was identified on the basis of local field potential (LFP) signals and single-unit spike patterns. Once the tetrodes were adjacent to the cell layer, they were settled into the cell layer for stable recordings.

Electrophysiological recording

Before recordings, the rats were again trained to perform the same tasks as those learned during the presurgery period. In some cases, the training was performed with the recording headstage and cable attached so that the rats became familiar with the recording condition. After confirmation that the rats again reached the criterion performance (> 95% correct) in the task, electrophysiological data collection commenced. Electrophysiological data were sampled at 2 kHz and filtered between 0.1 and 500 Hz. Unit activity was amplified and processed with a 750 Hz high-pass filter. Spike waveforms above a trigger threshold (–50 μV) were time-stamped and recorded at 30 kHz for 1.6 ms. Recordings were conducted for at least 2 days.

Muscimol injection

For muscimol injections, the dummy cannulas were removed from the guide cannulas and replaced by plastic injection cannulas with a diameter of 0.35 mm so that the tips of the injection cannulas were located above the hippocampus. The other side of the injection cannula was connected by polyethylene tubing to a 5 μL syringe mounted in a syringe pump. Then, through the injection cannula, 0.1 mg/ml muscimol dissolved in 0.9% NaCl solution was infused into the hippocampus at a rate of 0.2 μl/min for 5.0–7.5 min. After the infusion was completed, the injection cannula was left in place for 30 min, and the dummy cannula was again inserted into the guide tube. For control experiments, 1.0–1.5 μL of saline (0.9% NaCl) was injected with the same procedure. The behavioral test and recordings commenced more than 1 h after the injection. The spatial distribution of muscimol was estimated by infusion of 0.5 μg/μl sulforhodamine (SR101) in PBS at a rate of 0.2 μl/min for 5 min. During the injection procedure, the rats did not show any sign of stress or discomfort.

Random foraging task

On some recording days, the rats performed a random foraging task after 10–20-min resting periods after the 5-min task or the novel 5-min task. In the foraging task, rats were then placed in a 70-cm-sided square open field and allowed to freely forage for randomly scattered food pellets for 15 min. The rats were trained for the foraging task several times before recordings were acquired, and recordings in the foraging task were obtained in a familiar condition, termed a familiar foraging task. As shown in Figures S6D and S6E,

Please cite this article in press as: Shikano et al., Minute-encoding neurons in hippocampal-striatal circuits, Current Biology (2021), https://doi.org/10.1016/j.cub.2021.01.032

a recording in the foraging task was obtained for the first time, termed a novel foraging task, a similar condition to that reported in Tsao et al.[30].

Histological analysis to confirm electrode placement or cannula placement

The rats that received an overdose of urethane, were intracardially perfused with 4% paraformaldehyde in PBS and decapitated. To aid the reconstruction of electrode tracks, the electrodes were not withdrawn from the brain for more than 3 h after perfusion. After dissection, the brains were fixed overnight in 4% paraformaldehyde (PFA) and then equilibrated with a sequence of 20% sucrose and 30% sucrose in PBS. Frozen coronal sections (50 μm) were cut using a microtome (Sliding Microtome, SM2010 R, Leica Biosystems, Wetzlar, Germany), and serial sections were mounted and processed for cresyl violet staining. For cresyl violet staining, the slices were rinsed in water, counterstained with cresyl violet, and coverslipped with hydrophobic mounting medium (PARAmount-D). The positions of all tetrodes were confirmed by identifying the corresponding electrode tracks in histological tissue.

QUANTIFICATION AND STATISTICAL ANALYSIS

Spike sorting

Spike sorting was performed offline using the graphical cluster-cutting software MClust[58]. Recordings during rest periods before and after the behavioral paradigms were included in the analysis to assure recording stability throughout the experiment and to identify hippocampal cells that were silent during behavior. Clustering was performed manually in two-dimensional projections of the multi-dimensional parameter space (i.e., comparisons were made between waveform amplitudes, the peak-to-trough amplitude differences, and waveform energies; each aspect was measured on the four channels of each tetrode). Units with spike amplitudes of 100 μV and twice the baseline were detected offline by identifying clusters defined by waveform parameters. Cluster quality was measured by computing the L_{ratio} and isolation distance[59]. A cluster was considered as a cell when the L_{ratio} was less than 0.30 and the isolation distance was more than 14. Autocorrelation and cross-correlation functions were used as additional separation criteria. Refractory periods of spikes were considered to increase confidence in the successful isolation of cells. Hippocampal and striatal neurons with an average firing rate of more than 3 Hz and 10 Hz, respectively, were excluded from the analysis.

Analysis of behavioral patterns

For each session, changes in the probability of checking behavior during the 5-min intervals were computed from all success trials in each 10 s time bin. The temporal information TI_{check} was computed as follows[20]:

$$TI_{peek} = \sum_{i=1}^{N} P_i \frac{CP_i}{CP_{total}} \log_2 \frac{CP_i}{CP_{total}}$$

where CP_i is the probability of checking behavior at time bin i, CP_{total} is the total, and P_i is the probability that the rat was in time bin i (constant value = 1/30). To evaluate the significance of temporal information, the same analysis was applied to shuffled data in which the timing of checking behavior was randomly shuffled while maintaining the individual intercheck behavior intervals and the individual duration of intercheck behavior intervals in each trial. This randomization was repeated 1000 times, and a TI_{check} value was computed from each shuffled data point. A z-scored TI_{check} (zTI_{check}) was computed based on the TI_{check} distribution of the 1000 shuffled datasets. A zTI_{check} value greater than 2.33 ($p < 0.01$) was considered significant.

In addition, the same data were fitted by a linear regression line, and the slope of changes in checking behavior was defined when the p value was less than 0.01. For comparison across different sessions and rats, the slope was normalized by the average checking behavior over the session.

Chewing behavior was estimated from chewing-induced electrical noise recorded from an electrode placed on the neocortical surface (Figure S1J).

Analysis of temporal spike patterns

For each cell, a temporal firing-rate distribution was constructed by averaging spike rates across all success trials in individual time bins (10 s). The distributions were then smoothed with a Gaussian filter with a standard deviation of 1 (= 10 s), termed a temporal tuning curve for visualization (Figures 2, 4, and S2). In Figure 5, temporal tuning curves for single trials were constructed and smoothed with a Gaussian filter with a standard deviation of 3 (= 30 s).

Similar to zTI_{check}, we computed temporal information on spike patterns (TI_{spike}) for each cell. As rat positions, running speed, and peek behavior varied depending on elapsed time (Figures 1B and S1G), temporal components independent of these variables needed to be extracted from a temporal tuning curve. For this compensation, we employed the linear-nonlinear-Poisson (LN) model (for details, see Hardcastle et al.[29]) (Figures 2C and 4B, bottom). Briefly, average probabilities of rat positions (in a total of 4 bins, 12.5 × 12.5-cm^2 each), average probabilities of checking behavior (in a total of 4 bins, 25% each), average probabilities of running speed (in a total of 11 bins, 5 cm/s each), and average probability of elapsed time in the 5-min intervals (in a total of 30 bins, 10 s each) were computed in each 1 s time window across all trials. Using these behavioral variables, original spike-rate datasets (bin = 1 s) were

Please cite this article in press as: Shikano et al., Minute-encoding neurons in hippocampal-striatal circuits, Current Biology (2021), https://doi.org/10.1016/j.cub.2021.01.032

subject to the LN model. An LN model-based temporal tuning curve was defined as a sequence of modulation indexes of the time component (bin = 10 s). For visualization, an LN model-based temporal tuning curve was smoothed with a Gaussian filter with a standard deviation of 1 (= 10 s) (Figures 2, 4, and S2).

For a neuron showing spikes in more than 75% of trials, a temporal information TI_{spike} was computed as follows[20]:

$$TI_{spike} = \sum_{i=1}^{N} P_i \frac{MI_i}{MI_{total}} \log_2 \frac{MI_i}{MI_{total}}$$

where MI_i is the modulation index at time bin i, MI_{total} is the total modulation index, and P_i is the probability that the rat was in that time bin i (constant value = 1/15). To evaluate the significance of the temporal information, the same analysis was applied to shuffled data in which all interspike intervals were shuffled while keeping the total number of spikes in individual trials. This randomization was repeated 100 times, and a TI_{spike} value was computed from each shuffled data point. A z-scored TI_{spike} (zTI_{spike}) was computed based on the distribution of the TI_{spike} of 100 shuffled datasets. A minute-encoding neuron was defined if its average firing rate was within a certain range (hippocampus, from 0.1 to 3 Hz; striatum, from 0.1 to 10 Hz) and zTI_{spike} was greater than 2.33 ($p < 0.01$).

To determine firing types of each minute-encoding neuron, a regression line was computed by linearly fitting the bottom 50% of an LN model-adjusted temporal tuning curve that excluded the effect of a specific peak, if any. Minute-encoding neurons with a *P*-value less than 0.05 in the regression were considered significant and classified as a ramping firing type. Ramping up and down types were defined when these neurons had a significantly positive and negative regression slope, respectively. Second, a ridge-to-background (RB) ratio was computed[31,32]. If a neuron was classified as a ramping firing type, to exclude the effect of ramping, a tuning curve was compensated by subtracting the regression line from the LN model-adjusted temporal tuning curve. In all neurons tested, a tuning curve was normalized so that the maximum and minimum values were 1 and 0, respectively. In a normalized tuning curve, an RB ratio was computed with a ridge length of ~50 s and background periods that were more than 50 s from the peak. An RB ratio was then converted to a z-scored RB ratio (zRB ratio) based on the average and standard deviation of RB ratios computed from the corresponding 100 shuffled tuning curves in which modulation indexes in the original curve were randomized across time. Minute-encoding neurons with a zRB ratio higher than 2.33 ($p < 0.01$) were classified as a specific peak firing type. For a neuron classified as a specific peak firing type, a peak time was defined as the time bin corresponding to the center of the ridge. The range of a time field was defined as the time bins giving MIs higher than $min + 0.5 \times (max\text{-}min)$ Hz, where *max* and *min* represent the maximum and minimum MIs, respectively.

To analyze the sequentiality of tuning curves of minute-encoding neurons, all LN model-adjusted temporal tuning curves were normalized so that the maximum and minimum modulation indexes were 1 and 0, respectively, in each neuron. In a pooled dataset from all minute-encoding neurons identified (Figure 3E), a sequentiality index (SI) was computed as the sum of the entropy of the peak firing time distribution of minute-encoding neurons and the average logarithm of RB ratios of the neurons[31], where the entropy was computed as follows:

$$Entropy = \sum_{i=1}^{N} -p_i \log p_i$$

where i is the index of the bins (10 cm) of the tuning curve and p_i is the probability of the peak time of a minute-encoding neuron being at bin i. For comparisons, a perfect sequential (PS) model was constructed by assuming that the RB ratio of all neurons was 2.5, similar to the original data, and the peak firing time of these neurons was distributed completely uniformly across all time bins. A perfect ramping (PR) model was constructed by assuming that the tuning curves of all neurons showed a ramping up firing type.

In Figure 5, TI_{spike} was computed from a single trial, as described above, except that a 10 s time bin and a Gaussian kernel filter with a standard deviation of 3 were used. In Figure 5, zTI_{spike} was separately computed for each 5-min or 8-min condition. The calculation was performed from the original temporal tuning curves (bin = 10 s) without filtering.

Trial-to-trial variability of spike counts in time-encoding neurons

The trial-by-trial variability of spike patterns in minute-encoding neurons was compared with that of second-encoding neurons reported in Pastalkova et al.,[12] downloaded from the CRCNS data sharing website (hc-5; https://crcns.org/),[33] and in MacDonald et al.,[13] obtained from personal communications. The datasets included spike patterns of hippocampal neurons as rats ran on a running wheel for 15 s followed by left-side running (Pastalkova's datasets) or waited in a delay zone for < 10 s (MacDonald's datasets), in which time-encoding spike patterns in the range of seconds were observed (Figures S4A and S4B). For each cell, a raster plot of spike patterns aligned to trial onset was constructed from 10 randomly selected trials, and a temporal tuning curve was computed from the raster plot with a total number of bins of 30 (bin = 0.5 s or 0.17–0.27 s), the same as minute-encoding neurons. From each tuning curve, zTI_{spike} was computed, and neurons with zTI_{spike} greater than 2.33 were considered second-encoding neurons (Figure S4D, left). Each second-encoding neuron was classified into a specific peak firing type or a nonspecific peak firing type based on its zRB ratio, similar to minute-encoding neurons. For specific peak firing type neurons, the total number of spikes within a time field in each trial was counted, and a coefficient of variation ($CV_{in\text{-}field}$) of the spike counts was computed (Figure S4E, left). For nonspecific peak firing type neurons, the total number of spikes throughout an entire period in each trial was counted, and a coefficient of variation (CV_{entire}) of the spike counts was computed (Figure S4E, right).

Please cite this article in press as: Shikano et al., Minute-encoding neurons in hippocampal-striatal circuits, Current Biology (2021), https://doi.org/10.1016/j.cub.2021.01.032

Bayesian decoding of elapsed time

Naive Bayes classifiers were constructed by the MATLAB function. For each rat, spike patterns of all minute-encoding neurons and neurons with zTI_{spike} greater than 1.04 (Figures 3G–3I, 4I, and S5F–S5I) and elapsed time were set as predictors and response variables, respectively. Only success trials were included in the analysis. As the number of success trials varied across the rats, ranging from 11-19 trials, we randomly chose 10 success trials in each animal to create a classifier so that the numbers of trials in all rats used for decoding were equivalent (a cross-validation scheme). To decode time for a single target success trial (e.g., trial #1), a classifier was created from the other randomly selected 10 success trials. Next, to decode time for the next single target success trial (e.g., trial #2), a different classifier was created from the other randomly selected 10 success trials, meaning that classifiers differed every decoding process. This procedure was repeated for all single success trials. Sessions with more than three neurons were analyzed. Given that temporal tuning curves of spike rates (30 s bins) of n neurons were $SR_1, \ldots, SR_n$, the posterior probability of time T_i was calculated as:

$$P\left(T_i|SR_1, \ldots, SR_n\right) = \frac{P\left(T_i\right) P\left(SR_1, \ldots, SR_n|T_i\right)}{P\left(SR_1, \ldots, SR_n\right)}$$

In each time bin, a decoded time for each bin was defined as the time giving the highest posterior probability. The decoding error was computed as the sum of the absolute differences between real and predicted times from all trials. Errors at chance level were calculated from 100 shuffled datasets in which the time-firing rate relationship was randomized.

Scaling factor for the 5/8-min task

The temporal scaling property of checking behavior and spike patterns between the 5-min and 8-min conditions in the 5/8-min task was quantified by the best temporal scaling factor, similar to a previous study[40]. Temporal tuning curves were calculated from the percentage of checking behavior or spike rates (10 s bins, a Gaussian kernel filter with a standard deviation of 1). A behavioral tuning curve of the percentage of checking behavior in the 5 min condition was expressed as $CP_{5min}(T)$, where T was a series of timestamp t, consisting of 30 bins. A behavioral tuning curve of the percentage of checking behavior in the 8 min condition was upsampled 15 times by linearly connecting between a pair of neighboring bins, which was expressed as $CP_{8min}(T')$, where T' was a series of timestamp t', consisting of 753 (15 × 47 + 48) bins. A 5-min tuning curve, $CP_{5min}(T)$, was linearly expanded or compressed in time with scaling factors *Scale* ranging from 0.50 to 3.00 at an increment of 0.01. At each scaling factor, a scaled tuning curve $CP_{5min}(T \times Scale)$ was constructed. For each time point, $t \times Scale$, in the scaled tuning curve, the closest time point t' in $CP_{8min}(T')$ was identified and $CP_{8min}(t \times Scale)$ was approximated as $CP_{8min}(t')$. This computation was applied for all time points, $T \times Scale$, and $CP_{8min}(T \times Scale)$ was constructed. When *Scale* was more than 1.6, time points exceeding 8 min were excluded from the analysis. At each scaling factor, a mean square error (MSE) was computed between $CP_{5min}(T \times Scale)$ and $CP_{8min}(T \times Scale)$. The same analysis was applied to spike tuning curves. The best scaling factor of checking behavior (best SF_{check}) and spike rate (best SF_{spike}) was defined as the scaling factor that yielded the minimum MSE.

GLM fitting throughout a recording session

Similar to the analysis used in a previous study[30], a Poisson generalized linear model (GLM) was fitted to firing rate changes (bin = 10 s, without any smoothing) over a recording session for each cell. The variables used to fit the model for the 5-min task were trial time (bin = 10 s from 0 s to 300 s), session time (bin = 10 s from 0 s to 5450 s, including all success, omission, and miss trials, and 3 s pellet presentation periods), position (bin = 12.5 × 12.5 cm^2, a total of 4 bins), and the percentage of checking behavior (bin = 25% from 0% to 100%). With these variables, firing rates in individual time bins (bin = 10 s) were estimated by the MATLAB stepwise function (stepwiseglm.m). This function automatically computed an adjusted R^2 for each variable. An adjusted R^2 of more than 0.01 or less than 0.005 was used for the criterion to add or remove variables, respectively.

For GLM fitting for random foraging data, session time (bin = 10 s from 0 s to 900 s) and position (bin = 11.7 × 11.7 cm^2, a total of 36 bins) were included as variables.

Statistical analysis

All data are presented as the mean ± standard error of the mean (SEM) and were analyzed using MATLAB. Comparisons of two sample data (n = 44 or less samples) were analyzed by paired t test or Student's t test. Multiple group comparisons were performed by the statistical tests followed by Bonferroni corrections. Comparisons of two or more distributions were analyzed by the Kolmogorov-Smirnov test. Statistically significant temporal changes were assessed by one-way repeated-measures ANOVA (Figures 1C, 5C, and 5D). The null hypothesis was rejected when $p < 0.05$.